Numerical Model Reduction with error estimation for computational homogenization of non-linear consolidation

Citation for the original published paper (version of record):
Ekre, F., Larsson, F., Runesson, K. et al (2022). Numerical Model Reduction with error estimation for computational homogenization of non-linear consolidation. Computer Methods in Applied Mechanics and Engineering, 389.
http://dx.doi.org/10.1016/j.cma.2021.114334

Available online at www.sciencedirect.com
ScienceDirect
Comput. Methods Appl. Mech. Engrg. 389 (2022) 114334
Computer methods in applied mechanics and engineering
www.elsevier.com/locate/cma

Numerical Model Reduction with error estimation for computational homogenization of non-linear consolidation

Fredrik Ekre[a,*], Fredrik Larsson[a], Kenneth Runesson[a], Ralf Jänicke[b]

[a] Department of Industrial and Materials Science, Chalmers University of Technology, SE-41296 Gothenburg, Sweden
[b] Institute of Applied Mechanics, Technische Universität Braunschweig, 38106 Braunschweig, Germany

Received 5 July 2021; received in revised form 1 November 2021; accepted 6 November 2021
Available online 29 November 2021

Abstract

Numerical Model Reduction (NMR) is adopted for solving the non-linear microscale problem that arises from computational homogenization of a model problem of porous media with displacement and pressure as unknown fields. A reduced basis is obtained for the pressure field using Proper Orthogonal Decomposition and the pertinent displacement basis is obtained using Nonuniform Transformation Field Analysis. An explicit, fully computable, a posteriori error estimator is derived based on the linearized error equation for quantification of the NMR error in terms of a suitably chosen energy norm. The performance of the error estimates is demonstrated via a set of numerical examples with varying load amplitudes.

Keywords: Computational homogenization; Error control; Model reduction

1. Introduction

Computational homogenization using the so-called "Finite Element squared" (FE^2) procedure, cf. Feyel et al. [1], is a known approach to multiscale modeling where the constitutive relation is replaced with subscale computations carried out on Representative Volume Elements (RVE). The main advantage of FE^2, compared to a fully resolved solution, is the reduced computational cost, while still taking small scale processes or structures into account. However, the FE^2 scheme can still be very computationally demanding for practical problems since the number of RVE problems rapidly increases with the macroscale mesh density. It is therefore of interest to investigate methods to reduce the computational cost of solving the individual RVE problems.

A number of Numerical Model Reduction[1] (NMR) methods have been proposed for reducing the solution space of a discrete RVE problem. Many strategies are based on superposition of characteristic "modes". Waseem et al. [2] and Aggestam et al. [3] presented reduced models for computational homogenization of linear transient heat flow based on Spectral Decomposition (SD). Another example is the "eigendeformation-based reduced-order

* Corresponding author.
E-mail address: fredrik.ekre@chalmers.se (F. Ekre).

[1] The terms Reduced Order Modeling (ROM) and Model Order Reduction (MOR) are also used frequently in literature. We have chosen to use the term Numerical Model Reduction (NMR) to emphasize that we are using numerical methods to reduce the numerical problem, rather than tampering with the underlying model.

https://doi.org/10.1016/j.cma.2021.114334

homogenization" technique introduced by Fish and coworkers [4,5], which relies on the concept of Transformation Field Analysis (TFA) [6]. A similar approach, Nonuniform Transformation Field Analysis (NTFA), were presented by Michel and Suquet [7,8]. Fritzen et al. [9–12] combined NTFA with Proper Orthogonal Decomposition (POD) for visco-elasticity. Jänicke et al. [13] applied this approach to poroelasticity, whereby the pore pressure acts similar to inelastic strains in the NTFA framework. The result of applying the reduced model to the RVE problem(s) is that the macroscale problem reduces to a single-phase continuum with the "mode coefficients" as internal variables. The same POD-base reduction model is considered in this paper. Other reduction techniques have been studied in the context of multiscale finite element methods by e.g. Nguyen [14] for parametrized PDEs and by Efendiev et al. [15,16] for flows in heterogeneous media. A related topic is the concept of "hyperreduction", which has also been investigated for multiscale methods by, for example, Hernández et al. [17] and Memarnahavandi et al. [18], where, in addition to reducing of the number of degrees of freedom, also the cost for evaluating the residual is reduced. Reduced integration is, however, not considered in this paper.

Application of the reduced basis induces an error in addition to other modeling errors and the error inherent to the underlying (FE) discretization. In order to verify results from the reduced model it is of interest to control and quantify this error. Different error estimators have been developed in the context of multiscale modeling for different model reduction techniques. For example, methods for estimating the error from POD type reduction techniques have been presented by Abdulle et al. [19,20] for heterogeneous multiscale methods and by Boyaval [21] for numerical homogenization. Ohlberger and Schindler [22] developed a method for estimating the error for localized reduced basis multiscale methods. Error estimation based on the constitutive relation error have been proposed by Kerfriden et al. [23] and Chamoin and Legoll [24]. For the estimator proposed in this paper, we focus entirely on estimation of the NMR error and consider the fully resolved finite element solution to be the exact one, cf. e.g. Aggestam et al. [3] and Ekre et al. [25,26].

In this paper, we consider a continuum mechanics model of porous media as the model problem, cf. e.g. Jänicke et al. [13] but with non-linear permeability. We construct a reduced basis for the microscale problem using POD. The main contribution of this paper is the derivation of an explicit error estimator for estimation of the error stemming from the reduced basis. The estimate is based on the linearized version of the error equation together with an auxiliary symmetric form, cf. e.g. Pares et al. [27–29] which serves as an approximate bound. From the auxiliary form we obtain error bounds based on the discrete residual, cf. e.g. Jakobsson et al. [30]. We aim to base the estimate on the "active" modes, i.e. only the modes used for the reduced solution, and will thus not consider hierarchical approaches (e.g. by computing additional modes used solely for the purpose of estimating the error).

Throughout this paper, regular font is used to denote scalars (e.g. α), bold italic font is used to denote first and second order tensors (e.g. $\boldsymbol{u}$, $\boldsymbol{\varepsilon}$), and bold font to denote fourth order tensors (e.g. $\boldsymbol{\mathcal{E}}$). The scalar product (single contraction) is denoted with '$\cdot$', double contraction is denoted with ':' and the outer product is denoted with '$\otimes$'. For first order tensors $\boldsymbol{a}$, $\boldsymbol{b}$, second order tensor $\boldsymbol{A}$ and fourth order tensor $\boldsymbol{\mathcal{B}}$, we thus have

$$\boldsymbol{a} \cdot \boldsymbol{b} = a_i b_i, \tag{1a}$$

$$(\boldsymbol{A} \cdot \boldsymbol{b})_i = A_{ij} b_j, \tag{1b}$$

$$(\boldsymbol{\mathcal{B}} : \boldsymbol{A})_{ij} = B_{ijkl} A_{kl}, \tag{1c}$$

$$(\boldsymbol{a} \otimes \boldsymbol{b})_{ij} = a_i b_j, \tag{1d}$$

for Cartesian components, where repeated indices are summed over (Einstein summation convention). A superposed dot is used for time derivatives (e.g. $\dot{u} = \frac{\mathrm{d}u}{\mathrm{d}t}$). Volume averaging of a field $\bullet$ is denoted as

$$\langle \bullet \rangle_\square \coloneqq \frac{1}{|\Omega_\square|} \int_{\Omega_\square} \bullet \, \mathrm{d}\Omega, \tag{2}$$

where $\Omega_\square$ is the domain occupied by an RVE, and $|\Omega_\square|$ the corresponding volume.

The remainder of this paper is outlined as follows: Section 2 introduces computational homogenization for the model problem of porous media and defines the RVE problem, Section 3 introduces numerical model reduction (NMR) applied to the microscale (RVE) problem(s), Section 4 presents an error estimator for the NMR error in terms of an energy norm, Section 5 presents numerical examples demonstrating the behavior and effectivity of the estimator, and finally the paper is concluded in Section 6 with a summary and outlook for future work.

2. Two-scale analysis based on computational homogenization

2.1. The model problem - strong and space–time weak formats

As a model problem we consider a continuum mechanics description of a linear-elastic porous medium, where the pores are filled with a viscous fluid. We base our model on Jänicke et al. [13] which adapts Biot's equations for linear consolidation [31,32], with displacement $\boldsymbol{u} = \boldsymbol{u}(\boldsymbol{x}, t)$ and pressure $p = p(\boldsymbol{x}, t)$ as the primary fields

$$-\boldsymbol{\sigma}(\boldsymbol{u}, p) \cdot \boldsymbol{\nabla} = \boldsymbol{0} \qquad \forall \boldsymbol{x} \in \Omega \times (0, T], \tag{3a}$$

$$\dot{\Phi}(\boldsymbol{u}, p) + \boldsymbol{\nabla} \cdot \boldsymbol{w}(\boldsymbol{\nabla} p) = 0 \qquad \forall \boldsymbol{x} \in \Omega \times (0, T], \tag{3b}$$

where $\boldsymbol{\sigma}$ is the Cauchy stress tensor, Φ the fluid storage function and $\boldsymbol{w}$ the seepage velocity. The two fields are subjected to standard boundary conditions on the Dirichlet ($\Gamma_{\mathrm{D}}^{(u|p)}$) and Neumann ($\Gamma_{\mathrm{N}}^{(u|p)}$) parts of the boundary, respectively

$$\boldsymbol{u} = \boldsymbol{u}^{\mathrm{pres}} \quad \text{on } \Gamma_{\mathrm{D}}^{(u)} \times (0, T], \quad \boldsymbol{t} := \boldsymbol{\sigma} \cdot \boldsymbol{n} = \boldsymbol{t}^{\mathrm{pres}} \quad \text{on } \Gamma_{\mathrm{N}}^{(u)} \times (0, T], \tag{4a}$$

$$p = p^{\mathrm{pres}} \quad \text{on } \Gamma_{\mathrm{D}}^{(p)} \times (0, T], \quad h := \boldsymbol{w} \cdot \boldsymbol{n} = h^{\mathrm{pres}} \quad \text{on } \Gamma_{\mathrm{N}}^{(p)} \times (0, T]. \tag{4b}$$

We consider linear constitutive relations for the stress, and fluid storage. The stress is given by

$$\boldsymbol{\sigma} = \boldsymbol{E} : \boldsymbol{\varepsilon}[\boldsymbol{u}] - \alpha p \boldsymbol{I}, \tag{5}$$

where $\boldsymbol{E}$ is the constant elastic stiffness tensor, $\boldsymbol{\varepsilon}[\boldsymbol{u}] = [\boldsymbol{u} \otimes \boldsymbol{\nabla}]^{\mathrm{s}}$ is the linear strain tensor and α is the Biot coefficient. The storage function and seepage velocity for the liquid phase are given by

$$\Phi = \phi + \alpha \boldsymbol{\nabla} \cdot \boldsymbol{u} + \beta p, \tag{6a}$$

$$\boldsymbol{w} = -\boldsymbol{K} \cdot \boldsymbol{\nabla} p, \tag{6b}$$

where ϕ is the (initial) porosity, $\boldsymbol{K}$ is the permeability tensor, and β is the effective compressibility parameter of the fluid-filled pore space. α and β can be estimated in terms of the bulk moduli of the fluid, K^{f}, and the solid, K^{s}, phase as follows:

$$\alpha = 1 - \frac{K}{K^{\mathrm{s}}}, \tag{7a}$$

$$\beta = \frac{\phi}{K^{\mathrm{f}}} + \frac{\alpha - \phi}{K^{\mathrm{s}}}. \tag{7b}$$

In previous papers [13,26] the permeability tensor $\boldsymbol{K}$ has been constant. In this paper, however, we consider a non-linear formulation and let $\boldsymbol{K}$ depend on the volumetric part of the strain, viz.

$$\boldsymbol{K}(\boldsymbol{\nabla} \cdot \boldsymbol{u}) := f(\boldsymbol{\nabla} \cdot u)\boldsymbol{K}_0, \qquad f(\boldsymbol{\nabla} \cdot u) := \frac{1}{\alpha_0^2}\big(\alpha_0 + \boldsymbol{\nabla} \cdot \boldsymbol{u}\big)^2, \tag{8}$$

where α_0 is a material parameter, and where $\boldsymbol{K}_0 = k\boldsymbol{I}$ is a reference permeability.

Remark. In the limit $\alpha_0 \to \infty$ we obtain the classical linear formulation $\boldsymbol{K} \to \boldsymbol{K}_0$. □

Finally we need an initial condition for Φ, viz.

$$\Phi|_{t=0} = \Phi_0 = \phi + \alpha \boldsymbol{\nabla} \cdot \boldsymbol{u}_0 + \beta p_0. \tag{9}$$

The standard weak format in space–time, corresponding to (3), reads: Find $(\boldsymbol{u}, p) \in \mathcal{U} \times \mathcal{P}$ such that

$$\int_I \int_\Omega \Big[\boldsymbol{\varepsilon}[\boldsymbol{v}] : \boldsymbol{E} : \boldsymbol{\varepsilon}[\boldsymbol{u}] - \boldsymbol{\nabla} \cdot \boldsymbol{v}\ \alpha p\Big]\, \mathrm{d}\Omega \mathrm{d}t = \int_I \int_{\Gamma_{\mathrm{N}}} \boldsymbol{v} \cdot \boldsymbol{t}^{\mathrm{pres}}\, \mathrm{d}\Gamma \mathrm{d}t \quad \forall \boldsymbol{v} \in \mathcal{V}, \tag{10a}$$

$$\int_I \int_\Omega \Big[q\beta\, \dot{p} + \boldsymbol{\nabla} q \cdot \boldsymbol{K}(\boldsymbol{\nabla} \cdot \boldsymbol{u}) \cdot \boldsymbol{\nabla} p + \boldsymbol{\nabla} \cdot \dot{\boldsymbol{u}}\ \alpha q\Big]\, \mathrm{d}\Omega \mathrm{d}t + \int_\Omega [q\, \Phi]|_{t=0}\, \mathrm{d}\Omega = \int_I \int_{\Gamma_{\mathrm{N}}} q h^{\mathrm{pres}}\, \mathrm{d}\Gamma \mathrm{d}t + \int_\Omega [q\, \Phi_0]|_{t=0}\, \mathrm{d}\Omega \quad \forall q \in \mathcal{Q}. \tag{10b}$$

The semi-discrete version of (10) is obtained by defining

$$\mathbb{U}(t) \coloneqq \{\boldsymbol{v} \in \mathbb{U}_\mathrm{h} : \ \boldsymbol{v} = \boldsymbol{u}^\mathrm{pres} \text{ on } \Gamma_\mathrm{D}^{(u)}\}, \tag{11a}$$

$$\mathbb{U}^0 \coloneqq \{\boldsymbol{v} \in \mathbb{U}_\mathrm{h} : \ \boldsymbol{v} = \boldsymbol{0} \text{ on } \Gamma_\mathrm{D}^{(u)}\}, \tag{11b}$$

$$\mathbb{P}(t) \coloneqq \{q \in \mathbb{P}_\mathrm{h} : \ q = p^\mathrm{pres} \text{ on } \Gamma_\mathrm{D}^{(p)}\}, \tag{11c}$$

$$\mathbb{P}^0 \coloneqq \{q \in \mathbb{P}_\mathrm{h} : \ q = 0 \text{ on } \Gamma_\mathrm{D}^{(p)}\}, \tag{11d}$$

where $\mathbb{U}_\mathrm{h} \in [H^1(\Omega)]^3$ and $\mathbb{P}_\mathrm{h} \in H^1(\Omega)$ represents the finite element discretization, and H^1 the space of functions with square integrable derivatives of order 0 and 1. The spaces used in (10) are consequently defined as

$$\mathcal{U} \coloneqq H^1(I; \mathbb{U}(t)), \tag{12a}$$

$$\mathcal{V} \coloneqq L_2(I; \mathbb{U}^0), \tag{12b}$$

$$\mathcal{P} \coloneqq H^1(I; \mathbb{P}(t)), \tag{12c}$$

$$\mathcal{Q} \coloneqq \{q(\boldsymbol{x}, t) : \ q|_{t=0} \in \mathbb{P}^0, \ q|_I \in L_2(I; \mathbb{P}^0)\}. \tag{12d}$$

Here, we introduced Bochner spaces for space–time functions, such that, e.g., $H^1(I; X) = \{v(\boldsymbol{x}, t) : \ \|v(\bullet, t)\|_X \in H^1(I)\}$ and $L_2(I; X) = \{v(\boldsymbol{x}, t) : \ \|v(\bullet, t)\|_X \in L_2(I)\}$ for a space X of spatial functions with suitable norm $\|\bullet\|_X$. $L_2(I)$ and $H^1(I)$ are the spaces of square integrable functions and functions of square integrable derivatives, respectively, on the time interval I.

Remark. In order to shorten notation, we henceforth adopt the convention that the trace is included in $H^1(I)$, meaning that e.g., $q \in H^1(I; \mathbb{X})$ infers that $q(0)$ and $q(T)$ exist and reside in $\mathbb{X}$. □

2.2. First order selective homogenization in the spatial domain

The single-scale problem in Section 2.1 is replaced by a two-scale problem. We introduce (i) running averages in the weak form and (ii) scale separation via first order selective homogenization, following Larsson et al. [33]. As a first step we replace the single-scale problem (10) with the following, two-scale, problem: Find $(\boldsymbol{u}, p) \in \mathcal{U}_{\mathrm{FE}^2} \times \mathcal{P}_{\mathrm{FE}^2}$ such that

$$A^{(u)}(\boldsymbol{u}, p; \boldsymbol{v}) - L^{(u)}(\boldsymbol{v}) = 0 \qquad \forall \boldsymbol{v} \in \mathcal{V}_{\mathrm{FE}^2}, \tag{13a}$$

$$A^{(p)}(\boldsymbol{u}, p; q) - L^{(p)}(q) = 0 \qquad \forall q \in \mathcal{Q}_{\mathrm{FE}^2}, \tag{13b}$$

where the space–time variational forms are defined as

$$A^{(u)}(\boldsymbol{v}, q; \boldsymbol{w}) \coloneqq \int_I \int_\Omega \left[\mathfrak{a}_\square^{(u)}(\boldsymbol{v}, \boldsymbol{w}) - \mathfrak{b}_\square(q, \boldsymbol{w})\right] \mathrm{d}\Omega \mathrm{d}t, \tag{14a}$$

$$L^{(u)}(\boldsymbol{w}) \coloneqq \int_I \int_{\Gamma_\mathrm{N}} \boldsymbol{w} \cdot \boldsymbol{t}^\mathrm{pres} \, \mathrm{d}\Gamma \mathrm{d}t, \tag{14b}$$

$$A^{(p)}(\boldsymbol{v}, q; r) \coloneqq \int_I \int_\Omega \left[\mathfrak{m}_\square(\dot{q}, r) + \mathfrak{a}_\square^{(p)}(q, \boldsymbol{v}; r) + \mathfrak{b}_\square(r, \dot{\boldsymbol{v}})\right] \mathrm{d}\Omega \mathrm{d}t + \int_\Omega \left[\mathfrak{m}_\square(q, r) + \mathfrak{b}_\square(r, \boldsymbol{v})\right]\Big|_{t=0} \mathrm{d}\Omega, \tag{14c}$$

$$L^{(p)}(r) \coloneqq \int_I \int_{\Gamma_\mathrm{N}} r h^\mathrm{pres} \, \mathrm{d}\Gamma \mathrm{d}t + \int_\Omega \left[\mathfrak{m}_\square(p_0, r) + \mathfrak{b}_\square(r, \boldsymbol{u}_0)\right]\Big|_{t=0} \mathrm{d}\Omega. \tag{14d}$$

In (14) we introduced pertinent space-variational RVE-forms, representing running averages on domains $\Omega_\square$ located at each macroscale spatial point $\bar{\boldsymbol{x}}$:

$$\mathfrak{a}_\square^{(u)}(\boldsymbol{v}, \boldsymbol{w}) \coloneqq \langle \boldsymbol{\varepsilon}[\boldsymbol{w}] : \boldsymbol{E} : \boldsymbol{\varepsilon}[\boldsymbol{v}] \rangle_\square, \tag{15a}$$

$$\mathfrak{b}_\square(q, \boldsymbol{v}) \coloneqq \langle \nabla \cdot \boldsymbol{v} \ \alpha \ q \rangle_\square, \tag{15b}$$

$$\mathfrak{m}_\square(q, r) \coloneqq \langle r \beta q \rangle_\square, \tag{15c}$$

$$\mathfrak{a}_\square^{(p)}(q, \boldsymbol{v}; r) \coloneqq \langle \nabla r \cdot \boldsymbol{K}(\nabla \cdot \boldsymbol{v}) \cdot \nabla q \rangle_\square. \tag{15d}$$

In order to define the two-scale trial spaces $\mathcal{U}_{\mathrm{FE}^2}$, $\mathcal{P}_{\mathrm{FE}^2}$ and the corresponding test spaces $\mathcal{V}_{\mathrm{FE}^2}$, $\mathcal{Q}_{\mathrm{FE}^2}$, we introduce first order homogenization. However, to simplify matters we adopt *selective* homogenization, in the sense that it is

only the displacement field $\boldsymbol{u}$ that is decomposed into macroscale and microscale parts, whereas p is represented only as a fluctuation field. Hence, in each RVE, centered at macroscale coordinate $\bar{\boldsymbol{x}}$, we thus decompose $\boldsymbol{u}$ as

$$\boldsymbol{u}(\bar{\boldsymbol{x}};\boldsymbol{x},t) = \boldsymbol{u}^{\mathrm{M}}(\bar{\boldsymbol{x}};\boldsymbol{x},t) + \boldsymbol{u}^{\mu}(\bar{\boldsymbol{x}};\boldsymbol{x},t), \quad (\boldsymbol{x},t) \in \Omega_{\square} \times I, \tag{16}$$

where we use first order homogenization for the macroscale part, viz.

$$\boldsymbol{u}^{\mathrm{M}}(\bar{\boldsymbol{x}};\boldsymbol{x},t) := \bar{\boldsymbol{u}}(\bar{\boldsymbol{x}},t) + \bar{\boldsymbol{\varepsilon}}(\bar{\boldsymbol{x}},t)\cdot[\boldsymbol{x}-\bar{\boldsymbol{x}}], \tag{17}$$

with $\bar{\boldsymbol{\varepsilon}} := [\bar{\boldsymbol{u}} \otimes \nabla]^{\mathrm{s}}$. As to the pressure field we have

$$p(\bar{\boldsymbol{x}};\boldsymbol{x},t) = p^{\mu}(\bar{\boldsymbol{x}};\boldsymbol{x},t), \quad (\boldsymbol{x},t) \in \Omega_{\square} \times I, \tag{18}$$

i.e., the pressure field "lives" entirely on the subscale.

Remark. In view of the two-scale parametrization, the integrals for, e.g., $A^{(u)}$ in Eq. (14) should be interpreted as

$$A^{(u)}(\boldsymbol{v},q;\boldsymbol{w}) = \int_I \int_{\bar{\Omega}} \frac{1}{|\Omega_{\square}|} \int_{\Omega_{\square}} \boldsymbol{\varepsilon}[\delta\boldsymbol{u}(\bar{\boldsymbol{x}};\boldsymbol{x},t)] : \boldsymbol{\sigma}(\boldsymbol{u}(\bar{\boldsymbol{x}};\boldsymbol{x},t),\, p(\bar{\boldsymbol{x}};\boldsymbol{x},t))\,\mathrm{d}\Omega\mathrm{d}\bar{\Omega}\mathrm{d}t, \tag{19}$$

where consequently the RVE forms are parametrized with $\bar{\boldsymbol{x}}$, e.g., $\mathfrak{a}^{(u)}_{\square}(\bullet,\bullet) = \mathfrak{a}^{(u)}_{\square}(\bullet,\bullet)\{\bar{\boldsymbol{x}}\}$. □

We are now in the position to define the two-scale ansatz and test spaces

$$\mathcal{U}_{\mathrm{FE}^2} := \left\{ \boldsymbol{u} :\ \boldsymbol{u}|_{\Omega_{\square}} = \boldsymbol{u}^{\mathrm{M}}[\bar{\boldsymbol{u}}] + \boldsymbol{u}^{\mu},\ \boldsymbol{u}|_{\Gamma^{(u)}_{\mathrm{N}}} = \bar{\boldsymbol{u}},\ \boldsymbol{u}^{\mu} \in \mathcal{U}^{\mu}_{\square},\ \bar{\boldsymbol{u}} \in \bar{\mathcal{U}} \right\}, \tag{20a}$$

$$\mathcal{V}_{\mathrm{FE}^2} := \left\{ \boldsymbol{v} :\ \boldsymbol{v}|_{\Omega_{\square}} = \boldsymbol{v}^{\mathrm{M}}[\bar{\boldsymbol{v}}] + \boldsymbol{v}^{\mu},\ \boldsymbol{v}|_{\Gamma^{(u)}_{\mathrm{N}}} = \bar{\boldsymbol{v}},\ \boldsymbol{v}^{\mu} \in \mathcal{V}^{\mu}_{\square},\ \bar{\boldsymbol{v}} \in \bar{\mathcal{V}} \right\}, \tag{20b}$$

$$\mathcal{P}_{\mathrm{FE}^2} := \left\{ p :\ p|_{\Omega_{\square}} = p^{\mu},\ p^{\mu} \in \mathcal{P}_{\square} \right\}, \tag{20c}$$

$$\mathcal{Q}_{\mathrm{FE}^2} := \left\{ q :\ q|_{\Omega_{\square}} = q^{\mu},\ q^{\mu} \in \mathcal{Q}_{\square} \right\}, \tag{20d}$$

cf. Ekre et al. [25]. The details of the ansatz and test spaces in (20) are discussed in sections 2.3 and 2.4.

2.3. The macroscale (homogenized) problem

The macroscale problem is obtained from Eq. (13) by setting $\boldsymbol{v}^{\mu} = \boldsymbol{0}$ and $q^{\mu} = 0$. Find $\bar{\boldsymbol{u}} \in \bar{\mathcal{U}}$ such that

$$\int_I \int_{\Omega} \boldsymbol{\varepsilon}[\bar{\boldsymbol{v}}] : \bar{\boldsymbol{\sigma}}(\bar{\boldsymbol{u}}, \boldsymbol{u}^{\mu})\,\mathrm{d}\Omega\mathrm{d}t = \int_I \int_{\Gamma_{\mathrm{N}}} \bar{\boldsymbol{v}} \cdot \boldsymbol{t}^{\mathrm{pres}}\,\mathrm{d}\Gamma\mathrm{d}t \quad \forall \bar{\boldsymbol{v}} \in \bar{\mathcal{V}}, \tag{21}$$

where $\bar{\mathcal{U}}$ and $\bar{\mathcal{V}}$ are the ansatz and test spaces for the macroscale problem. We omit the exact definitions of these spaces, since we henceforth in this paper focus solely on the local microscale RVE-problem. The homogenized stress $\bar{\boldsymbol{\sigma}}$ is defined as

$$\bar{\boldsymbol{\sigma}}\{\boldsymbol{\varepsilon}[\bar{\boldsymbol{u}}]\} := \langle \boldsymbol{\sigma} \rangle_{\square}, \tag{22}$$

where $\bar{\boldsymbol{\sigma}}\{\bar{\boldsymbol{\varepsilon}}\}$ is implicit due to the history dependence.

2.4. The microscale (RVE) problem

Since we shall (in this paper) be concerned only with the solution of the RVE-problem, we consider the situation where $\boldsymbol{u}^{\mathrm{M}}$ from (17) is known, i.e. $\bar{\boldsymbol{u}}(t)$ and $\bar{\boldsymbol{\varepsilon}}(t)$ are known functions in time (for the given RVE in question). The problem (13) thus reduces to that of finding $(\boldsymbol{u}^{\mu}, p) \in \mathcal{U}^{\mu}_{\square} \times \mathcal{P}_{\square}$ that solve

$$A^{(u)}_{\square}(\boldsymbol{u}^{\mu}, p; \boldsymbol{v}^{\mu}) = 0 \qquad \forall \boldsymbol{v}^{\mu} \in \mathcal{V}^{\mu}_{\square}, \tag{23a}$$

$$A^{(p)}_{\square}(\boldsymbol{u}^{\mu}, p; q) - L^{(p)}_{\square}(q) = 0 \qquad \forall q \in \mathcal{Q}_{\square}, \tag{23b}$$

where we introduced the RVE space–time variational forms

$$A^{(u)}_{\square}(\boldsymbol{v},q;\boldsymbol{w}) := \int_I \Big[\mathfrak{a}^{(u)}_{\square}(\boldsymbol{u}^{\mathrm{M}} + \boldsymbol{v}, \boldsymbol{w}) - \mathfrak{b}_{\square}(q, \boldsymbol{w}) \Big] \mathrm{d}t, \tag{24a}$$

$$A_{\square}^{(p)}(\boldsymbol{v}, q; r) := \int_I \Big[\mathfrak{m}_{\square}(\dot{q}, r) + \mathfrak{a}_{\square}^{(p)}(q, \boldsymbol{u}^{\mathrm{M}} + \boldsymbol{v}; r) + \mathfrak{b}_{\square}(r, \dot{\boldsymbol{u}}^{\mathrm{M}} + \dot{\boldsymbol{v}}) \Big] \mathrm{d}t + \Big[\mathfrak{m}_{\square}(q, r) + \mathfrak{b}_{\square}(r, \boldsymbol{u}^{\mathrm{M}} + \boldsymbol{v}) \Big] \Big|_{t=0}, \tag{24b}$$

$$L_{\square}^{(p)}(r) := \Big[\mathfrak{m}_{\square}(p_0, r) + \mathfrak{b}_{\square}(r, \boldsymbol{u}_0) \Big] \Big|_{t=0}. \tag{24c}$$

We adopt Dirichlet boundary conditions, for both $\boldsymbol{u}^{\mu}$ and p, and the spaces of spatial functions for the RVE problem are consequently defined as

$$\mathbb{U}_{\square}^0 := \{ \boldsymbol{v} \in \mathbb{U}_{\square,\mathrm{h}} : \ \boldsymbol{v} = \boldsymbol{0} \text{ on } \Gamma_{\square} \}, \tag{25a}$$

$$\mathbb{P}_{\square} := \{ q \in \mathbb{P}_{\square,\mathrm{h}} : \ q = 0 \text{ on } \Gamma_{\square} \}, \tag{25b}$$

where $\mathbb{U}_{\square,\mathrm{h}}$ and $\mathbb{P}_{\square,\mathrm{h}}$ are the (spatially) FE-discretized function spaces. The trial and test spaces in (23) can be expressed as

$$\mathcal{U}_{\square}^{\mu} := H^1(I; \mathbb{U}_{\square}^0), \tag{26a}$$

$$\mathcal{V}_{\square}^{\mu} := L_2(I; \mathbb{U}_{\square}^0), \tag{26b}$$

$$\mathcal{P}_{\square} := H^1(I; \mathbb{P}_{\square}), \tag{26c}$$

$$\mathcal{Q}_{\square} := \{ q(\boldsymbol{x}, t) : \ q|_{t=0} \in \mathbb{P}_{\square}, \ q|_I \in L_2(I; \mathbb{P}_{\square}) \}. \tag{26d}$$

3. Numerical Model Reduction

In this Section we present the NMR procedure for establishing the reduced version of the RVE problem in Eq. (23). The Section is organized as follows: Section 3.1 introduces an alternative formulation of Eq. (23) utilizing that Eq. (23a) is time invariant, Section 3.2 introduces the NMR-ansatz of p and $\boldsymbol{u}^{\mu}$ based on spatial modes, Section 3.3 presents the explicit reduced RVE problem, Section 3.4 discusses the mode identification strategy, Section 3.5 defines a projection operator onto the reduced space (used for error estimation, cf. Section 4), and Section 3.6 summarizes the NMR strategy.

3.1. Preliminaries

We will now use the fact that Eq. (23a) is time-invariant, and does not contain any time derivatives, of $\boldsymbol{u}$ or p, to reduce the problem further. As a preliminary step we introduce an implicit reduction of the displacement fluctuation $\boldsymbol{u}^{\mu}$. For any $t \in I$ we define

$$\boldsymbol{u}^{\mu}(t) = \boldsymbol{u}_{\bar{\boldsymbol{\varepsilon}}}^{\mu}(t) + \boldsymbol{u}_p^{\mu}\{p(t)\}, \tag{27}$$

where $\boldsymbol{u}_{\bar{\boldsymbol{\varepsilon}}}^{\mu}(t) \in \mathbb{U}_{\square}^0$ satisfies

$$\mathfrak{a}_{\square}^{(u)}(\boldsymbol{u}_{\bar{\boldsymbol{\varepsilon}}}^{\mu}(t), \delta\boldsymbol{u}^{\mu}) = \mathfrak{a}_{\square}^{(u)}(-\boldsymbol{u}^{\mathrm{M}}(t), \delta\boldsymbol{u}) \qquad \forall \delta\boldsymbol{u}^{\mu} \in \mathbb{U}_{\square}^0, \tag{28}$$

and the implicit function $\boldsymbol{u}_p^{\mu}$ is defined from

$$\boldsymbol{u}_p^{\mu}\{q\} := \boldsymbol{u}_p^{\mu} \in \mathbb{U}_{\square}^0 : \ \mathfrak{a}_{\square}^{(u)}(\boldsymbol{u}_p^{\mu}, \delta\boldsymbol{u}) = \mathfrak{b}_{\square}(q, \delta\boldsymbol{u}) \qquad \forall \delta\boldsymbol{u} \in \mathbb{U}_{\square}^0. \tag{29}$$

In summary, for a given RVE, we use the following decomposition of $\boldsymbol{u}$

$$\boldsymbol{u} = \boldsymbol{u}^{\mathrm{M}} + \boldsymbol{u}^{\mu} = \underbrace{\boldsymbol{u}^{\mathrm{M}} + \boldsymbol{u}_{\bar{\boldsymbol{\varepsilon}}}^{\mu}}_{=:\boldsymbol{u}_{\bar{\boldsymbol{\varepsilon}}}} + \boldsymbol{u}_p^{\mu} = \boldsymbol{u}_{\bar{\boldsymbol{\varepsilon}}} + \boldsymbol{u}_p^{\mu}. \tag{30}$$

Remark. We note, from (28), that $\boldsymbol{u}_{\bar{\boldsymbol{\varepsilon}}}^{\mu}$ can be directly assessed in terms of unit strain perturbations, i.e.

$$\boldsymbol{u}_{\bar{\boldsymbol{\varepsilon}}}^{\mu}(\boldsymbol{x}, t) = \sum_{i,j=1}^{n_{\mathrm{dim}}} \hat{\boldsymbol{u}}_{\bar{\boldsymbol{\varepsilon}}}^{(i,j)}(\boldsymbol{x}) \bar{\boldsymbol{\varepsilon}}(t) : [\boldsymbol{e}_i \otimes \boldsymbol{e}_j], \tag{31}$$

where the "unit fields" $\hat{\boldsymbol{u}}_{\bar{\boldsymbol{\varepsilon}}}^{(i,j)} (= \hat{\boldsymbol{u}}_{\bar{\boldsymbol{\varepsilon}}}^{(j,i)}) \in \mathbb{U}_{\square}^0$ are solved from

$$\mathfrak{a}_{\square}^{(u)}(\hat{\boldsymbol{u}}_{\bar{\boldsymbol{\varepsilon}}}^{(i,j)}, \delta\boldsymbol{u}^{\mu}) = -\mathfrak{a}_{\square}^{(u)}(\boldsymbol{e}_i \otimes \boldsymbol{e}_j \cdot [\boldsymbol{x} - \bar{\boldsymbol{x}}], \delta\boldsymbol{u}^{\mu}) \qquad \forall \delta\boldsymbol{u}^{\mu} \in \mathbb{U}_{\square}^0 \qquad i, j = 1, 2, \ldots, n_{\mathrm{dim}}. \tag{32}$$

□

With the displacement fluctuation implicitly known from p we can formulate a condensed version of the original problem in (23): Find $p \in \mathcal{P}_\square$ such that

$$A_\square(p, q) - L_\square(q) = 0 \qquad \forall q \in \mathcal{Q}_\square, \tag{33}$$

where we defined

$$A_\square(q, r) := \int_I \left[\mathfrak{m}_\square(\dot{q}, r) + \mathfrak{a}_\square(q; r) + \mathfrak{b}_\square(r, \dot{\boldsymbol{u}}_{\bar{\boldsymbol{\varepsilon}}} + \boldsymbol{u}_p^\mu\{\dot{q}\}) \right] \mathrm{d}t + \left[\mathfrak{m}_\square(q, r) + \mathfrak{b}_\square(r, \boldsymbol{u}_{\bar{\boldsymbol{\varepsilon}}} + \boldsymbol{u}_p^\mu\{q\}) \right]\Big|_{t=0}, \tag{34a}$$

$$L_\square(q) := \left[\mathfrak{m}_\square(p_0, q) + \mathfrak{b}_\square(q, \boldsymbol{u}_0) \right]\Big|_{t=0}, \tag{34b}$$

with

$$\mathfrak{a}_\square(q; r) := \mathfrak{a}_\square^{(p)}(q, \boldsymbol{u}_{\bar{\boldsymbol{\varepsilon}}} + \boldsymbol{u}_p^\mu\{q\}; r). \tag{35}$$

3.2. NMR-ansatz

We now introduce the concept of Numerical Model Reduction (NMR) with the aim to reduce the computational cost of solving each RVE problem (33). To this end we construct a reduced spatial basis for the pressure, and define $p_{\mathrm{R}}(\boldsymbol{x}, t)$ as the approximation of $p(\boldsymbol{x}, t)$ with an expansion using N_{R} modes

$$p(\boldsymbol{x}, t) \approx p_{\mathrm{R}}(\boldsymbol{x}, t) = \sum_{a=1}^{N_{\mathrm{R}}} p_a(\boldsymbol{x}) \xi_a(t) \in \mathcal{P}_{\square,\mathrm{R}} := H^1(I; \mathbb{P}_{\square,\mathrm{R}}), \tag{36}$$

where $\{p_a\}_{a=1}^{N_{\mathrm{R}}}$ is a set of linearly independent basis functions that span the reduced RVE space

$$\mathbb{P}_{\square,\mathrm{R}} := \mathrm{span}\{p_a\}_{a=1}^{N_{\mathrm{R}}} \subset \mathbb{P}_\square, \tag{37}$$

and where ξ_a are mode "activity coefficients". The identification of the spatial modes p_a will be discussed further in Section 3.4.

In order to satisfy (29), and find $\boldsymbol{u}_p^\mu\{p(t)\}$, we make the following ansatz

$$\boldsymbol{u}_{p,\mathrm{R}}^\mu(\boldsymbol{x}, t) = \sum_{a=1}^{N_{\mathrm{R}}} \boldsymbol{u}_a^\mu(\boldsymbol{x}) \xi_a(t) \tag{38}$$

where $\boldsymbol{u}_a^\mu(\boldsymbol{x})$ are (spatial) displacement modes and where $\xi_a(t)$ are the *same* mode activity coefficients as those used for the reduced pressure field. Due to linearity, the sequence of displacement modes can be solved from (29), i.e. find $\boldsymbol{u}_a^\mu = \boldsymbol{u}_p^\mu\{p_a\} \in \mathbb{U}_\square$ such that

$$\mathfrak{a}_\square^{(u)}(\boldsymbol{u}_a^\mu, \delta\boldsymbol{u}^\mu) = \mathfrak{b}_\square(p_a, \delta\boldsymbol{u}^\mu) \qquad \forall \delta\boldsymbol{u}^\mu \in \mathbb{U}_\square^0 \qquad a = 1, 2, \ldots, N_{\mathrm{R}}. \tag{39}$$

This corresponds to solving one stationary, linear, problem for each mode p_a. We note that there is no need to establish the full $\boldsymbol{u}_p^\mu\{q\} : \mathbb{P}_\square \to \mathbb{U}_\square^0$.

Remark. We note that there is no reduction of the balance of momentum equation, and the residual of Eq. (23a) is guaranteed to be zero. This follows from time invariance of Eq. (23a), the definition of the displacement field (Eqs. (30), (38)) and the definition of the modes $\boldsymbol{u}_a^\mu(x)$ solved from the corresponding pressure modes p_a (Eq. (39)). □

3.3. Explicit form of the reduced subscale problem

With the approximations from the previous section we can, following the procedure in Jänicke et al. [13], define the reduced equivalent of (23): Find $p_{\mathrm{R}} \in \mathcal{P}_{\square,\mathrm{R}}$ such that

$$A_\square(p_{\mathrm{R}}, q_{\mathrm{R}}) - L_\square(q_{\mathrm{R}}) = 0 \qquad \forall q_{\mathrm{R}} \in \mathcal{Q}_{\square,\mathrm{R}}, \tag{40}$$

where $\mathcal{Q}_{\square,\mathrm{R}}$ follows from (26d), with $\mathbb{P}_\square$ replaced by $\mathbb{P}_{\square,\mathrm{R}}$. Hence, we can expand the test function q using the spatial pressure modes, i.e. $q_\mathrm{R} = \sum_{a=1}^{N_\mathrm{R}} p_a \eta_a$, and express (40) explicitly as the problem of finding the mode coefficients $\xi_b(t) \in H^1(I),\ b = 1, 2, \ldots, N_\mathrm{R}$ such that

$$\begin{aligned}
&\int_I \eta_a \Big[\mathfrak{m}_\square(\sum_{b=1}^{N_\mathrm{R}} p_b \dot{\xi}_b,\, p_a) + \mathfrak{a}_\square^{(p)}(\sum_{b=1}^{N_\mathrm{R}} p_b \xi_b,\, \boldsymbol{u}_{\bar{\boldsymbol{\varepsilon}}} + \sum_{b=1}^{N_\mathrm{R}} \boldsymbol{u}_b^\mu \xi_b;\, p_a) + \mathfrak{b}_\square(p_a,\, \dot{\boldsymbol{u}}_{\bar{\boldsymbol{\varepsilon}}} + \sum_{b=1}^{N_\mathrm{R}} \boldsymbol{u}_b^\mu \dot{\xi}_b) \Big] \mathrm{d}t + \\
&\eta_a(0) \Big[\mathfrak{m}_\square(\sum_{b=1}^{N_\mathrm{R}} p_b \xi_b,\, p_a) \xi_b + \mathfrak{b}_\square(p_a,\, \boldsymbol{u}_{\bar{\boldsymbol{\varepsilon}}} + \sum_{b=1}^{N_\mathrm{R}} \boldsymbol{u}_b^\mu \xi_b) \Big] \Big|_{t=0} - \eta_a(0) \Big[\mathfrak{m}_\square(p_0,\, p_a) + \mathfrak{b}_\square(p_a,\, \boldsymbol{u}_0) \Big] \Big|_{t=0} = 0 \\
&\quad \forall \eta_a \in \mathcal{X}, \quad a = 1, 2, \ldots, N_\mathrm{R},
\end{aligned} \tag{41}$$

where

$$\mathcal{X} := \{ v(t) :\ v|_{t=0} \in \mathbb{R},\ v|_I \in L_2(I) \}. \tag{42}$$

Eq. (41) can be formulated as a semi-discrete, non-linear, system of size N_R as follows

$$\underline{M}\, \dot{\underline{\xi}} + \underline{R}(\underline{\xi}) - \underline{f} = 0, \tag{43a}$$

$$\underline{M}\, \underline{\xi}^0 - \underline{f}^0 = 0, \tag{43b}$$

where $\underline{\xi}$ is the vector of unknowns, $\underline{\xi} = (\xi_1, \xi_2, \ldots, \xi_{N_\mathrm{R}})$, and where

$$(\underline{M})_{ab} = (\underline{M})_{ba} = \mathfrak{m}_\square(p_b,\, p_a) + \mathfrak{b}_\square(p_a,\, \boldsymbol{u}_b^\mu), \tag{44a}$$

$$(\underline{R})_a = \mathfrak{a}_\square^{(p)}(\sum_{b=1}^{N_\mathrm{R}} p_b(\underline{\xi})_b,\, \boldsymbol{u}_{\bar{\boldsymbol{\varepsilon}}} + \sum_{b=1}^{N_\mathrm{R}} \boldsymbol{u}_b^\mu(\underline{\xi})_b;\, p_a), \tag{44b}$$

$$(\underline{f})_a = \mathfrak{b}_\square(p_a, -\dot{\boldsymbol{u}}_{\bar{\boldsymbol{\varepsilon}}}) = \big[\sum_{ij}^{n_\mathrm{dim}} \mathfrak{b}_\square(p_a, -\boldsymbol{e}_i \otimes \boldsymbol{e}_j \cdot [\boldsymbol{x} - \bar{\boldsymbol{x}}] - \hat{\boldsymbol{u}}_{\bar{\boldsymbol{\varepsilon}}}^{(i,j)} \boldsymbol{e}_i \otimes \boldsymbol{e}_j) \big] : \dot{\bar{\boldsymbol{\varepsilon}}}, \tag{44c}$$

$$(\underline{f}^0)_a = \Big[\mathfrak{m}_\square(p_0,\, p_a) + \mathfrak{b}_\square(p_a,\, \boldsymbol{u}_0 - \boldsymbol{u}_{\bar{\boldsymbol{\varepsilon}}}) \Big] \Big|_{t=0}. \tag{44d}$$

Symmetry of $\underline{M}$ follows from symmetry of $\mathfrak{m}_\square(\bullet, \bullet)$, symmetry of $\mathfrak{a}_\square^{(u)}(\bullet, \bullet)$, and from the definition of the displacement modes in (39), i.e. $\mathfrak{b}_\square(p_a, \boldsymbol{u}_b^\mu) = \mathfrak{a}_\square^{(u)}(\boldsymbol{u}_a^\mu, \boldsymbol{u}_b^\mu) = \mathfrak{b}_\square(p_b, \boldsymbol{u}_a^\mu)$.

The full two-scale model involves the solution of (reduced) microscale problems (41), typically one for each macroscale quadrature point, in order to find homogenized stress $\bar{\boldsymbol{\sigma}}$ and the sensitivity w.r.t. the macroscale strain $\frac{\partial \bar{\boldsymbol{\sigma}}}{\partial \bar{\boldsymbol{\varepsilon}}}$. In particular, the homogenized stress can be formulated as

$$\bar{\boldsymbol{\sigma}}(t) = \bar{\boldsymbol{E}}_{\bar{\boldsymbol{\varepsilon}}} : \boldsymbol{\varepsilon}(t) + \sum_{a=1}^{N_\mathrm{R}} \bar{\boldsymbol{E}}_{p,a}\ \xi_a(t), \tag{45}$$

where the fourth order tensor $\bar{\boldsymbol{E}}_{\bar{\boldsymbol{\varepsilon}}}$ and the second order tensors $\bar{\boldsymbol{E}}_{p,a}$ can be computed in the "offline stage", resulting in efficient evaluation of the homogenized stress, i.e.

$$\bar{\boldsymbol{E}}_{\bar{\boldsymbol{\varepsilon}}} = \langle \boldsymbol{E} \rangle_\square + \sum_{ij}^{n_\mathrm{dim}} \langle \boldsymbol{E} : \boldsymbol{\varepsilon}[\hat{\boldsymbol{u}}_{\bar{\boldsymbol{\varepsilon}}}^{(i,j)}] \rangle_\square \boldsymbol{e}_i \otimes \boldsymbol{e}_j, \tag{46a}$$

$$\bar{\boldsymbol{E}}_{p,a} = \langle \boldsymbol{E} : \boldsymbol{\varepsilon}[\boldsymbol{u}_a^\mu] \rangle_\square - \langle p_a \rangle_\square \boldsymbol{I}, \tag{46b}$$

where $\boldsymbol{E}$ is the fourth order stiffness tensor for linear elasticity.

3.4. Identification of the reduced basis

In this section we discuss the procedure of constructing the reduced basis. In this paper we will use Proper Orthogonal Decomposition (POD), cf. Jänicke et al. [13], however there are other options. As an example, similar to Ekre et al. [26], it is possible to find a basis using Spectral Decomposition also for the nonlinear problem by (i) ignoring the coupling and (ii) using a constant permeability.

The POD basis is extracted from a dataset of spatial pressure "snapshots" collected during fully resolved training simulations where the RVE is subjected to prescribed macroscopic load meant to activate the typical behavior of the material. For a dataset of N_S snapshots $\hat{p}_k := p(t_k),\ k = 1, 2, \ldots, N_\mathrm{S}$ we first form the correlation matrix $\underline{C}$ with entries[2]

$$(\underline{C})_{kl} = \langle \hat{p}_k \hat{p}_l \rangle_\square \quad k, l = 1, 2, \ldots, N_\mathrm{S}. \tag{47}$$

The correlation matrix is used to solve the eigenvalue problem $\underline{C}\underline{\varphi} = \lambda\underline{\varphi}$, from which we obtain eigenvalues λ_a and eigenvectors $\underline{\varphi_a}$, ordered based on the eigenvalues in decreasing order such that $\lambda_1 \geq \lambda_2, \ldots$. The final modes, used for the reduced pressure solution, are computed as

$$p_a = \sum_{k=1}^{N_\mathrm{S}} \hat{p}_k (\underline{\varphi_a})_k, \quad a = 1, 2, \ldots, N_\mathrm{R}. \tag{48}$$

Remark. The number of modes N_R is determined by truncation of the eigenvalues series, in practice when the quotient λ_N/λ_1 becomes "sufficiently small". □

3.5. Projection onto the reduced space

For the subsequent error analysis we define a projection operator $\Pi_\mathrm{R} : L_2(\Omega_\square) \to \mathbb{P}_{\square,\mathrm{R}}$ such that, for any given $q \in L_2(\Omega_\square)$ and for any given reduced set $\mathbb{P}_{\square,\mathrm{R}}$, the projection $\Pi_\mathrm{R} q \in \mathbb{P}_{\square,\mathrm{R}}$ is defined by the following identity

$$\mathfrak{m}_\square(\Pi_\mathrm{R} q, \delta q) = \mathfrak{m}_\square(q, \delta q) \qquad \forall \delta q \in \mathbb{P}_{\square,\mathrm{R}}. \tag{49}$$

We also define the complementary operator

$$\Pi_\mathrm{C} := \mathrm{I} - \Pi_\mathrm{R} \tag{50}$$

where I is the identity operator. We note that for $p, q \in L_2(\Omega_\square)$ the following identity holds

$$\mathfrak{m}_\square(p, \Pi_\mathrm{C} q) = \mathfrak{m}_\square(\Pi_\mathrm{C} p, q) \tag{51}$$

since

$$\begin{aligned} &\mathfrak{m}_\square(p, \Pi_\mathrm{C} q) \overset{(50)}{=} \mathfrak{m}_\square(p, q) - \mathfrak{m}_\square(p, \Pi_\mathrm{R} q) \overset{(49)}{=} \\ &\quad \mathfrak{m}_\square(p, q) - \mathfrak{m}_\square(\Pi_\mathrm{R} p, \Pi_\mathrm{R} q) \overset{(49)}{=} \mathfrak{m}_\square(p, q) - \mathfrak{m}_\square(\Pi_\mathrm{R} p, q) \overset{(50)}{=} \mathfrak{m}_\square(\Pi_\mathrm{C} p, q). \end{aligned} \tag{52}$$

3.6. Summary of NMR procedure

The NMR procedure is summarized in Fig. 1 where we highlight the following steps corresponding to the figure:

1. Training simulations solving Eq. (23) with representative loading while capturing pressure snapshots;
2. Computation of pressure modes $p_a(\boldsymbol{x})$ based on snapshot POD (Eq. (48)), and the corresponding displacement modes $\boldsymbol{u}_a^\mu(\boldsymbol{x})$ (Eq. (39));
3. Pre-computation of fixed quantities based on the modes used for the solution and error estimation (e.g. $\underline{M}$ and $\underline{f}$ for the discrete system (43));
4. Solution of the reduced system Eq. (43);
5. Estimation of the NMR error (see Section 4).

The figure also illustrates which steps can be performed in the offline stage and which steps belong to the online stage.

[2] Another common approach is to define the entries as the scalar product of the "nodal values", i.e. $(\underline{C})_{kl} = \underline{\hat{p}}_k^\mathrm{T}\ \underline{\hat{p}}_l$, where $\underline{\hat{p}}_k$ and $\underline{\hat{p}}_l$ are vectors containing the finite element representation of $\hat{p}_k$ and $\hat{p}_l$, respectively.

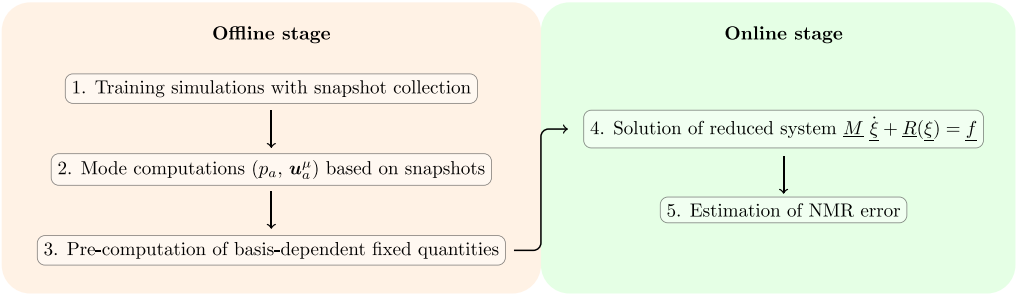

Fig. 1. Schematic illustration of the major steps for establishing the reduced RVE problem.

4. Estimation of the NMR error

The reduced solution based on the reduced basis is an approximation of the exact solution, which is an extra source of error in addition to e.g. space- and time-discretization errors, model errors, etc. In what follows we ignore errors stemming from other sources, and focus solely on the error introduced by NMR, by considering the solution to the fully resolved (finite element) problem to be exact.

We define the exact error in the pressure as

$$g_{\text{ex}}(\boldsymbol{x}, t) \coloneqq p(\boldsymbol{x}, t) - p_{\text{R}}(\boldsymbol{x}, t) \quad \in \mathcal{P}_\square, \tag{53}$$

where $p \in \mathcal{P}_\square$ is the exact solution, and where $p_{\text{R}} \in \mathcal{P}_{\square,\text{R}}$ is the reduced solution. Since the problem is non-linear the equation for solving the exact error is also non-linear. We will therefore base the error estimate on a linearized error equation.

The following building blocks are used in order to obtain the explicit error estimate:

- definition of the error and corresponding error equation (Section 4.1);
- definition of the approximate error solved from the linearized error equation (Section 4.1);
- definition of an auxiliary form and corresponding auxiliary error equation (Section 4.2);
- derivation of explicit estimates based on the auxiliary error equation (Section 4.3).

The steps of the procedure are summarized in Section 4.4.

4.1. Linearized error equation and residual

Formally, the exact error g_{ex} must be solved from the following (non-linear) equation:

$$A_\square(p_{\text{R}} + g_{\text{ex}}, q) - L(q) = 0 \quad \forall q \in \mathcal{Q}_\square. \tag{54}$$

For estimating the error we will use the linearized version of (54) and define the approximate error $g(\boldsymbol{x}, t) \approx g_{\text{ex}}(\boldsymbol{x}, t)$ which is solved from the following problem: Find $g(\boldsymbol{x}, t)$ s.t.

$$A_{\square,\text{R}}(g, q) = R_\square(q) \coloneqq L_\square(q) - A_\square(p_{\text{R}}, q) \quad \forall q \in \mathcal{Q}_\square, \tag{55}$$

where the linearized form is defined as follows

$$\begin{aligned} A_{\square,\text{R}}(g, q) &\coloneqq A'_\square(p_{\text{R}}; q, g) \coloneqq \left[\frac{\mathrm{d}}{\mathrm{d}\tau} A_\square(p_{\text{R}} + \tau g, q)\right]\Big|_{\tau=0} = \\ &\int_I \left[\mathfrak{m}_\square(\dot{g}, q) + \mathfrak{a}_{\square,\text{R}}(g, q) + \mathfrak{b}_\square(q, \boldsymbol{u}_p^\mu\{\dot{g}\})\right]\mathrm{d}t + \left[\mathfrak{m}_\square(g, q) + \mathfrak{b}_\square(q, \boldsymbol{u}_p^\mu\{g\})\right]\Big|_{t=0}, \end{aligned} \tag{56}$$

with

$$\begin{aligned} \mathfrak{a}_{\square,\text{R}}(g, q) &\coloneqq \mathfrak{a}'_\square(p_{\text{R}}; q, g) \coloneqq \left[\frac{\mathrm{d}}{\mathrm{d}\tau} \mathfrak{a}_\square(p_{\text{R}} + \tau g, q)\right]\Big|_{\tau=0} = \\ &\langle \nabla q \cdot \boldsymbol{K} \cdot \nabla g + \nabla q \cdot \boldsymbol{K}' \cdot \nabla p_{\text{R}}\, [\nabla \cdot \boldsymbol{u}_p^\mu\{g\}] \rangle_\square. \end{aligned} \tag{57}$$

The residual from Eq. (55) can be written explicitly as

$$
\begin{aligned}
R_\square(q) = L_\square(q) - A_\square(p_{\mathrm{R}}, q) = \Big[\mathfrak{m}_\square(p_0, q) + \mathfrak{b}_\square(q, \boldsymbol{u}_0)\Big]\Big|_{t=0} - \\
\int_I \Big[\mathfrak{m}_\square(\dot{p}_{\mathrm{R}}, q) + \mathfrak{a}_\square(p_{\mathrm{R}}; q) + \mathfrak{b}_\square(q, \dot{\boldsymbol{u}}_{\bar{\boldsymbol{\varepsilon}}} + \boldsymbol{u}_p^\mu\{\dot{p}_{\mathrm{R}}\})\Big]\mathrm{d}t - \Big[\mathfrak{m}_\square(p_{\mathrm{R}}, q) + \mathfrak{b}_\square(q, \boldsymbol{u}_{\bar{\boldsymbol{\varepsilon}}} + \boldsymbol{u}_p^\mu\{p_{\mathrm{R}}\})\Big]\Big|_{t=0} = \\
\int_I \Big[\mathfrak{m}_\square(-\dot{p}_{\mathrm{R}} - \frac{\alpha}{\beta}\nabla\cdot[\dot{\boldsymbol{u}}_{\bar{\boldsymbol{\varepsilon}}} + \boldsymbol{u}_p^\mu\{\dot{p}_{\mathrm{R}}\}], q) + \langle\nabla q\cdot\boldsymbol{K}\cdot\nabla p_{\mathrm{R}}\rangle_\square\Big]\mathrm{d}t \\
+\Big[\mathfrak{m}_\square(p_0 - p_{\mathrm{R}} + \frac{\alpha}{\beta}\nabla\cdot[\boldsymbol{u}_0 - \boldsymbol{u}_{\bar{\boldsymbol{\varepsilon}}} - \boldsymbol{u}_p^\mu\{p_{\mathrm{R}}\}], q)\Big]\Big|_{t=0} = \\
\int_I \Big[\mathfrak{m}_\square(M_t, q) + \langle\nabla q\cdot(-\boldsymbol{w}_t)\rangle_\square\Big]\mathrm{d}t + \Big[\mathfrak{m}_\square(M_0, q)\Big]\Big|_{t=0},
\end{aligned}
\tag{58}
$$

where we defined

$$
M_t := -\dot{p}_{\mathrm{R}} - \frac{\alpha}{\beta}\nabla\cdot[\dot{\boldsymbol{u}}_{\bar{\boldsymbol{\varepsilon}}} + \boldsymbol{u}_p^\mu\{\dot{p}_{\mathrm{R}}\}], \tag{59a}
$$

$$
\boldsymbol{w}_t := -\boldsymbol{K}(\nabla\cdot[\boldsymbol{u}_{\bar{\varepsilon}} + \boldsymbol{u}_p^\mu\{p_{\mathrm{R}}\}])\cdot\nabla p_{\mathrm{R}}, \tag{59b}
$$

$$
M_0 := p_0 - p_{\mathrm{R}} + \frac{\alpha}{\beta}\nabla\cdot[\boldsymbol{u}_0 - \boldsymbol{u}_{\bar{\boldsymbol{\varepsilon}}} - \boldsymbol{u}_p^\mu\{p_{\mathrm{R}}\}]. \tag{59c}
$$

For the linear problem, cf. Ekre et al. [26], it is possible to parametrize the residual w.r.t. $\{\xi_a(t)\}_{a=1}^{N_{\mathrm{R}}}$ and $\bar{\varepsilon}(t)$ in time, and trivially define M_t to include also the contribution from $\boldsymbol{w}_t$ without requiring any extra work in the online stage. For this formulation, M_t and M_0 in (59) can be parametrized. However, due to the non-linearity, $\boldsymbol{w}_t$ cannot be parametrized in the same (low) order.

Since Eq. (40) is assumed to be solved exactly we note that

$$
R_\square(q_{\mathrm{R}}) = 0 \quad \forall q_{\mathrm{R}} \in \mathcal{Q}_{\square,\mathrm{R}}, \tag{60}
$$

whereby the following Galerkin-like orthogonality holds:

$$
R_\square(q) = R_\square(q) - R_\square(\Pi_{\mathrm{R}} q) = R_\square(\Pi_{\mathrm{C}} q) \quad \forall q \in \mathcal{Q}_\square. \tag{61}
$$

4.2. Auxiliary symmetric form and auxiliary error equation

We now define an auxiliary form with the requirements that it should (i) define a norm, (ii) localize in time, and (iii) (approximately) bound $A_{\square,\mathrm{R}}$ from below. We define $\hat{A}_\square(\bullet,\bullet)$ as follows:

$$
\hat{A}_\square(g, q) := \int_I \hat{\mathfrak{a}}_\square(g, q)\mathrm{d}t + \frac{1}{2}\mathfrak{m}_\square(g, q)|_{t=0} + \frac{1}{2}\mathfrak{m}_\square(g, q)|_{t=T}, \tag{62}
$$

where we also defined

$$
\hat{\mathfrak{a}}_\square(g, q) := \langle\nabla g\cdot\boldsymbol{K}_0\cdot\nabla q\rangle_\square. \tag{63}
$$

$\hat{A}_\square$ now defines the following global space–time norm

$$
\|q\| := \sqrt{\hat{A}_\square(q, q)} = \sqrt{\int_I \|q\|_{\mathfrak{a}}^2\mathrm{d}t + \frac{1}{2}\|q\|_{\mathfrak{m}}^2|_{t=0} + \frac{1}{2}\|q\|_{\mathfrak{m}}^2|_{t=T}} \tag{64}
$$

together with the spatial norms $\|\bullet\|_{\mathfrak{a}}$ and $\|\bullet\|_{\mathfrak{m}}$

$$
\|q\|_{\mathfrak{a}} := \sqrt{\hat{\mathfrak{a}}_\square(q, q)}, \qquad \|q\|_{\mathfrak{m}} := \sqrt{\mathfrak{m}_\square(q, q)}. \tag{65}
$$

As we discussed earlier the auxiliary form should be a lower bound of the true tangent $A_{\square,\mathrm{R}}$, i.e.

$$
\hat{A}_\square(q, q) \lesssim A'_\square(p_{\mathrm{R}}; q, q) = A_{\square,\mathrm{R}}(q, q). \tag{66}
$$

This approximation is motivated by the follow inequality for the limit $p \to 0$:

$$
\hat{A}_\square(q, q) \leq \lim_{p\,\to\,0} A'_\square(p; q, q), \tag{67}
$$

which holds for the auxiliary form, as defined by Eq. (62), since the bilinear form pertinent to the linearized problem

$$\begin{aligned}
&\lim_{p\to 0} A'_\square(p;q,q) = \int_I \Big[\mathfrak{m}_\square(\dot q,q) + \lim_{p\to 0}\mathfrak{a}'_\square(p;q,q) + \mathfrak{b}_\square(q,\boldsymbol{u}_p^\mu\{\dot q\})\Big]\mathrm{d}t + \\
&\Big[\mathfrak{m}_\square(q,q) + \mathfrak{b}_\square(q,\boldsymbol{u}_p^\mu\{q\})\Big]\Big|_{t=0} = \\
&\int_I \Big[\underbrace{\lim_{p\to 0}\mathfrak{a}'_\square(p;q,q)}_{=\hat{\mathfrak{a}}_\square(q,q)}\Big]\mathrm{d}t + \frac{1}{2}\Big[\mathfrak{m}_\square(q,q) + \underbrace{\mathfrak{b}_\square(q,\boldsymbol{u}_p^\mu\{q\})}_{\geq 0}\Big]\Big|_{t=0} + \frac{1}{2}\Big[\mathfrak{m}_\square(q,q) + \underbrace{\mathfrak{b}_\square(q,\boldsymbol{u}_p^\mu\{q\})}_{\geq 0}\Big]\Big|_{t=T} \geq \\
&\int_I \hat{\mathfrak{a}}_\square(q,q)\mathrm{d}t + \frac{1}{2}\mathfrak{m}_\square(q,q)\big|_{t=0} + \frac{1}{2}\mathfrak{m}_\square(q,q)\big|_{t=T} = \hat{A}_\square(q,q),
\end{aligned} \tag{68}$$

where we used that (i) $\lim_{p\to 0}\mathfrak{a}'_\square(p;q,r) = \langle \nabla q \cdot \boldsymbol{K}_0 \cdot \nabla r\rangle_\square$, and (ii) $\mathfrak{b}_\square(q,\boldsymbol{u}_p^\mu\{q\}) = \mathfrak{a}_\square^{(u)}(\boldsymbol{u}_p^\mu\{q\},\boldsymbol{u}_p^\mu\{q\}) \geq 0$ from Eq. (39).

We now define the auxiliary error equation for an auxiliary error representation $\hat g$: Find $\hat g \in \mathcal{P}_\square$ such that

$$\hat A_\square(\hat g, q) = R_\square(q) = R_\square(\Pi_{\mathrm{C}} q) \quad \forall q \in \mathcal{Q}_\square, \tag{69}$$

where the right-hand side can be substituted due to the orthogonality property in (61). We note that the norm of the auxiliary error is an approximate upper bound on the true error, i.e. $\|g\| \lesssim \|\hat g\|$. This follows from the definition of the error equations, and the approximate bound from Eq. (66):

$$\|g\|^2 = \hat A_\square(g,g) \lesssim A_{\square,\mathrm{R}}(g,g) = R_\square(g) = \hat A_\square(\hat g, g) \leq \|\hat g\|\|g\|. \tag{70}$$

In summary, we obtain the estimator $\|g\| \lesssim \|\hat g\|$, where the bound is guaranteed in the limit of linear response, cf. Ekre et al. [26]. The bound can thus be considered reliable for moderate non-linearities. However, even for strong non-linearities, we remark that $\|\hat g\|$ reflects the full residual due to the coercivity of $\hat A_\square(\bullet,\bullet)$.

A more conservative estimate can be obtained by replacing the inequality from Eq. (67) with

$$\hat A_\square(q,q) \leq \frac{1}{f^-} A_{\square,\mathrm{R}}(q,q), \tag{71}$$

and finding an estimate for $f^- < 1$. This gives a bound that is valid also outside the limit $p \to 0$. In place of Eq. (70) we obtain

$$\|g\|^2 = \hat A_\square(g,g) \leq \frac{1}{f^-} A_{\square,\mathrm{R}}(q,q) = \frac{1}{f^-} R_\square(g) = \frac{1}{f^-}\hat A_\square(\hat g, g) \leq \frac{1}{f^-}\|\hat g\|\|g\|. \tag{72}$$

For the considered model problem, f^- could be estimated by considering Eq. (8) and let

$$f^- = \min_{t\in I,\ \boldsymbol{x}\in\Omega_\square} f(\nabla\cdot\boldsymbol{u}(\boldsymbol{x},t)). \tag{73}$$

Discarding the skew-symmetric term, we may assume

$$\mathfrak{a}'_\square(p_{\mathrm{R}};q,q) \geq f^-\ \hat{\mathfrak{a}}_\square(q,q), \tag{74}$$

which motivates Eq. (71).

4.3. Explicit estimate

We shall now derive an explicit, fully computable, estimate for the (approximate) error using the auxiliary error equation (69). From the definition of the norm we have

$$\|g\| \lesssim \|\hat g\| = \sqrt{\hat A_\square(\hat g,\hat g)} = \sqrt{\int_I \|\hat g\|_{\mathfrak{a}}^2\mathrm{d}t + \frac{1}{2}\|\hat g\|_{\mathfrak{m}}^2|_{t=0} + \frac{1}{2}\|\hat g\|_{\mathfrak{m}}^2|_{t=T}}. \tag{75}$$

Since the auxiliary error equation localizes in time we shall in the following three sections derive upper bounds on $\|\hat g\|_{\mathfrak{a}}^2$, $\|\hat g\|_{\mathfrak{m}}^2|_{t=0}$, and $\|\hat g\|_{\mathfrak{m}}^2|_{t=T}$, respectively. More specifically, upon considering (58) and (62) the problem in (69) localizes into one problem for $t=0$, one problem for each $t\in I$, and one problem for $t=T$.

4.3.1. Auxiliary error equation at time $t = 0$

At time $t = 0$ the auxiliary error equation is reduced to the following problem: Find $\hat{g}(0) =: \hat{g}_0 \in \mathbb{P}_\square$ such that

$$\frac{1}{2}\mathfrak{m}_\square(\hat{g}_0, q) = \mathfrak{m}_\square(M_0, \Pi_C q) \quad \forall q \in \mathbb{P}_\square. \tag{76}$$

Using the identity from (52), and Cauchy–Schwartz inequality, we obtain the following upper estimate

$$\|\hat{g}_0\|_{\mathfrak{m}}^2 = \mathfrak{m}_\square(\hat{g}_0, \hat{g}_0) = 2\mathfrak{m}_\square(M_0, \Pi_C \hat{g}_0) = \mathfrak{m}_\square(\Pi_C M_0, \hat{g}_0) \leq \|\Pi_C M_0\|_{\mathfrak{m}} \|\hat{g}_0\|_{\mathfrak{m}}, \tag{77}$$

which results in the following contribution to the global estimate in (75):

$$\frac{1}{2}\|\hat{g}(0)\|_{\mathfrak{m}}^2 \leq 2\|\Pi_C M_0\|_{\mathfrak{m}}^2. \tag{78}$$

Remark. If the initial condition can be represented exactly using the reduced basis, for example if $p(\bullet, 0) = 0$, then we obtain the trivial contribution $\frac{1}{2}\|\hat{g}(0)\|_{\mathfrak{m}}^2 \equiv 0$ since $M_0 \equiv 0$. □

4.3.2. Auxiliary error equation at time $t \in I$

In the time interval the auxiliary error equation reduces to the problem of finding $\hat{g}(t) =: \hat{g}_t \in \mathbb{P}_\square$ such that

$$\hat{\mathfrak{a}}_\square(\hat{g}_t, q) = \mathfrak{m}_\square(M_t, \Pi_C q) + \langle \nabla \Pi_C q \cdot (-\boldsymbol{w}_t) \rangle_\square \quad \forall q \in \mathbb{P}_\square. \tag{79}$$

As discussed previously, for the linear problem (Ekre et al. [26]) it is possible to parametrize the residual w.r.t. time, and trivially project the full residual into an effective M_t (whereby $\boldsymbol{w}_t = 0$) without requiring any extra work in the online stage. However, it is not possible to use that strategy for the non-linear problem since it would require the solution of a (linear) problem of size N at each timestep. Instead we will propose a different strategy for shifting data from $\boldsymbol{w}_t$ to M_t in Eq. (85) by using a decomposition of $\boldsymbol{w}_t$ using POD.

We first decompose $\boldsymbol{w}_t(\boldsymbol{x})$ at each time t as follows

$$\boldsymbol{w}_t(\boldsymbol{x}) = \hat{\boldsymbol{w}}_t(\boldsymbol{x}) + \boldsymbol{w}_t'(\boldsymbol{x}), \qquad \hat{\boldsymbol{w}}_t(\boldsymbol{x}) \in \mathbb{W}_\square := \sum_{a=1}^{M} \boldsymbol{w}_a(\boldsymbol{x}) \chi_a, \tag{80}$$

where $\mathbb{W}_\square := \text{span}\{\boldsymbol{w}_a(\boldsymbol{x})\}_{a=1}^M$ defines a spatial basis of M modes for the seepage, and where χ_a are the mode activity coefficients. The new basis functions $\boldsymbol{w}_a$ are obtained by employing POD (cf. Section 3.4) on a dataset of seepage snapshots collected during either the (original) offline training stage, or during the simulation itself. For each time t, $\hat{\boldsymbol{w}}_t$ is thus defined as the projection of $\boldsymbol{w}_t$ onto $\mathbb{W}_\square$. The M mode coefficients χ_a are solved from[3]

$$\langle \hat{\boldsymbol{w}}_t \cdot \boldsymbol{K}_0^{-1} \cdot \delta\hat{\boldsymbol{w}} \rangle_\square = \langle \boldsymbol{w}_t \cdot \boldsymbol{K}_0^{-1} \cdot \delta\hat{\boldsymbol{w}} \rangle_\square, \tag{81}$$

i.e. a linear problem of size $M \ll N$ for each timestep.

To shift $\hat{\boldsymbol{w}}$ into a contribution to $\mathfrak{m}_\square(\bullet, \bullet)$, we define $\Delta M_t \in \mathbb{P}_\square$ as the projection of $\hat{\boldsymbol{w}}_t$ onto $\mathbb{P}_\square$

$$\mathfrak{m}_\square(\Delta M_t, q) = \langle \nabla q \cdot (-\hat{\boldsymbol{w}}_t) \rangle_\square \quad \forall q \in \mathbb{P}_\square. \tag{82}$$

With the definition of ΔM_t and $\hat{\boldsymbol{w}}_t$ we can rewrite the residual in Eq. (79) as follows

$$\begin{aligned} &\mathfrak{m}_\square(M_t, q) + \langle \nabla q \cdot (-\boldsymbol{w}_t) \rangle_\square = \mathfrak{m}_\square(M_t, q) + \langle \nabla q \cdot (-\hat{\boldsymbol{w}}_t - \boldsymbol{w}_t') \rangle_\square = \\ &\quad \mathfrak{m}_\square(M_t + \Delta M_t, q) + \langle \nabla q \cdot (-\boldsymbol{w}_t') \rangle_\square = \mathfrak{m}_\square(M_t', q) + \langle \nabla q \cdot (-\boldsymbol{w}_t') \rangle_\square, \end{aligned} \tag{83}$$

where we defined $M_t' := M_t + \Delta M_t$. Finally, from linearity, $\Delta M_t := \sum_{a=1}^M M_{t,a} \chi_a$ where the spatial modes $M_{t,a} \in \mathbb{P}_\square$ can be solved from the seepage modes $\boldsymbol{w}_a$

$$\mathfrak{m}_\square(M_{t,a}, q) = \langle \nabla q \cdot (-\boldsymbol{w}_a) \rangle_\square \quad \forall q \in \mathbb{P}_\square, \quad a = 1, 2, \ldots, M. \tag{84}$$

The localized error equation (79) now gives the following contribution to the global norm

$$\|\hat{g}_t\|_{\mathfrak{a}}^2 = \hat{\mathfrak{a}}_\square(\hat{g}_t, \hat{g}_t) = \mathfrak{m}_\square(M_t', \Pi_C \hat{g}_t) + \langle \nabla \Pi_C \hat{g}_t \cdot (-\boldsymbol{w}_t') \rangle_\square. \tag{85}$$

[3] Ultimately we want to minimize $\boldsymbol{w}_t' = \boldsymbol{w}_t - \hat{\boldsymbol{w}}_t$ in terms of $\|\boldsymbol{w}_t'\|_{\boldsymbol{K}_0^{-1}} = \sqrt{\langle \boldsymbol{w}_t' \cdot \boldsymbol{K}_0^{-1} \cdot \boldsymbol{w}_t' \rangle_\square}$, and thus solve the coefficients from the corresponding stationary point.

The first term of (85) can be bounded using Cauchy–Schwartz inequality as follows

$$\mathfrak{m}_\square(M_t', \Pi_C \hat{g}_t) = \mathfrak{m}_\square(\Pi_C M_t', \hat{g}_t) \leq \|\Pi_C M_t'\|_\mathfrak{m} \|\hat{g}_t\|_\mathfrak{m}, \tag{86}$$

where the first identity follow from the orthogonality property of Π_C in (51). To proceed we need a relation between $\|\bullet\|_\mathfrak{m}$ and $\|\bullet\|_\mathfrak{a}$. To this end we define the following eigenvalue problem

$$\hat{\mathfrak{a}}_\square(\varphi_a, \delta p) = \lambda_a \mathfrak{m}_\square(\varphi_a, \delta p) \quad \forall \delta p \in \mathbb{P}_\square, \qquad a = 1, 2, \ldots, N, \tag{87a}$$

$$\mathfrak{m}_\square(\varphi_a, \varphi_b) = \delta_{ab} \qquad a = 1, 2, \ldots, N, \tag{87b}$$

where (φ_a, λ_a), $a = 1, 2, \ldots, N$ are eigenpairs ordered such that $\lambda_1 \leq \lambda_2 \leq \cdots \leq \lambda_N$. We can compose any $q \in \mathbb{P}_\square$ as follows

$$q = \sum_{a=1}^{N} \varphi_a \xi_a, \tag{88}$$

and obtain a relation between $\|\bullet\|_\mathfrak{m}$ and $\|\bullet\|_\mathfrak{a}$

$$\|q\|_\mathfrak{m}^2 = \sum_{a=1}^{N} \xi_a^2 = \sum_{a=1}^{N} \frac{\lambda_a \xi_a^2}{\lambda_a} \leq \frac{1}{\lambda_1} \sum_{a=1}^{N} \lambda_a \xi_a^2 = \frac{1}{\lambda_1} \hat{\mathfrak{a}}_\square(q, q) = \frac{1}{\lambda_1} \|q\|_\mathfrak{a}^2. \tag{89}$$

Combining (86) and (89) gives the following upper estimate for the first term of (85)

$$\mathfrak{m}_\square(M_t', \Pi_C \hat{g}) \leq \frac{1}{\sqrt{\lambda_1}} \|\Pi_C M_t'\|_\mathfrak{m} \|\hat{g}_t\|_\mathfrak{a}. \tag{90}$$

The second term of (85) can similarly be bounded, using Cauchy–Schwartz inequality, as follows:

$$\langle \nabla \Pi_C \hat{g}_t \cdot (-\boldsymbol{w}_t') \rangle_\square = \langle \nabla \Pi_C \hat{g}_t \cdot \boldsymbol{K}_0^{\frac{1}{2}} \cdot \boldsymbol{K}_0^{-\frac{1}{2}} \cdot (-\boldsymbol{w}_t') \rangle_\square \leq$$
$$\sqrt{\left\langle \nabla \Pi_C \hat{g}_t \cdot \boldsymbol{K}_0 \cdot \nabla \Pi_C \hat{g}_t \right\rangle} \sqrt{\left\langle \boldsymbol{w}_t' \cdot \boldsymbol{K}_0^{-1} \cdot \boldsymbol{w}_t' \right\rangle} = \|\Pi_C \hat{g}_t\|_\mathfrak{a} \|\boldsymbol{w}_t'\|_{\boldsymbol{K}_0^{-1}}, \tag{91}$$

where we defined

$$\|\bullet\|_{\boldsymbol{K}_0^{-1}} := \sqrt{\langle \bullet \cdot \boldsymbol{K}_0^{-1} \cdot \bullet \rangle_\square}. \tag{92}$$

As the last step we need to relate $\|\Pi_C \hat{g}_t\|_\mathfrak{a}$ to $\|\hat{g}_t\|_\mathfrak{a}$. A first, conservative, option is to use the identity operator in place of Π_C already in (85), since the right hand side of the residual can be substituted, cf. Eq. (61). In this case we directly obtain

$$\langle \nabla \hat{g}_t \cdot (-\boldsymbol{w}_t') \rangle_\square \leq \|\hat{g}_t\|_\mathfrak{a} \|\boldsymbol{w}_t\|_{\boldsymbol{K}_0^{-1}}. \tag{93}$$

Remark. This option requires that the identity operator is used in place of Π_C also in the bound for first term in Eq. (90). □

A second, approximate, option is to simply assume that $\|\Pi_C \hat{g}_t\|_\mathfrak{a} \leq \|\hat{g}_t\|_\mathfrak{a}$ which results in

$$\langle \nabla \Pi_C \hat{g}_t \cdot (-\boldsymbol{w}_t') \rangle_\square \lesssim \|\hat{g}_t\|_\mathfrak{a} \|\boldsymbol{w}_t'\|_{\boldsymbol{K}_0^{-1}}. \tag{94}$$

Combining the results from (90) and (93) or (94) with (85) we obtain the following upper bounds for the time-interval contribution

$$\|\hat{g}_t\|_\mathfrak{a} \leq \frac{\|M_t'\|_\mathfrak{m}}{\sqrt{\lambda_1}} + \|\boldsymbol{w}_t'\|_{\boldsymbol{K}_0^{-1}}, \qquad \|\hat{g}_t\|_\mathfrak{a} \lesssim \frac{\|\Pi_C M_t'\|_\mathfrak{m}}{\sqrt{\lambda_1}} + \|\boldsymbol{w}_t'\|_{\boldsymbol{K}_0^{-1}}. \tag{95}$$

4.3.3. Auxiliary error equation at time $t = T$

At time $t = T$ the auxiliary error equation is reduced to the following problem: Find $\hat{g}(T) =: \hat{g}_T \in \mathbb{P}_\square$ such that

$$\frac{1}{2} \mathfrak{m}_\square(\hat{g}_T, q) = 0 \quad \forall q \in \mathbb{P}_\square, \tag{96}$$

Table 1
Material parameters for the three material phases in the RVEs used for the numerical examples.

		Phase 1 (matrix)	Phase 2/3 (inclusions)
G	[GPa]	8.8	15.8
K	[GPa]	9.6	16.2
ϕ	[–]	0.2	0.1
K^{s}	[GPa]	36	36
K^{f}	[GPa]	0.022	2.3
k	[$\mathrm{m}^2\,\mathrm{MPa}^{-1}\,\mathrm{s}^{-1}$]	2	0.033/0.0033
α_0	[–]	0.2	0.2

which gives the following trivial contribution to the global norm:

$$\frac{1}{2}\|\hat{g}(T)\|_{\mathrm{m}}^2 \equiv 0. \tag{97}$$

4.3.4. Final estimate of NMR error

Eq. (75) together with Eqs. (78), (95), and (97) gives the following estimates of the auxiliary error

$$\begin{aligned}\|\hat{g}\| &\leq \sqrt{\int_I \|\hat{g}\|_{\mathrm{a}}^2 \mathrm{d}t + \frac{1}{2}\|\hat{g}\|_{\mathrm{m}}^2|_{t=0} + \frac{1}{2}\|\hat{g}\|_{\mathrm{m}}^2|_{t=T}} \quad = \\ &\begin{cases} \leq \sqrt{\int_I \left[\frac{\|M_t'\|_{\mathrm{m}}}{\sqrt{\lambda_1}} + \|\boldsymbol{w}_t'\|_{\boldsymbol{K}_0^{-1}}\right]^2 \mathrm{d}t + 2\|\Pi_{\mathrm{C}} M_0\|_{\mathrm{m}}^2} =: E_{\mathrm{est}}, \\ \lesssim \sqrt{\int_I \left[\frac{\|\Pi_{\mathrm{C}} M_t'\|_{\mathrm{m}}}{\sqrt{\lambda_1}} + \|\boldsymbol{w}_t'\|_{\boldsymbol{K}_0^{-1}}\right]^2 \mathrm{d}t + 2\|\Pi_{\mathrm{C}} M_0\|_{\mathrm{m}}^2} =: E_{\mathrm{est}}^{\Pi_{\mathrm{C}}}, \end{cases}\end{aligned} \tag{98}$$

where E_{est} is a guaranteed estimate, and $E_{\mathrm{est}}^{\Pi_{\mathrm{C}}}$ a sharper, but approximate, estimate of the auxiliary error. However, from (70) we know that both options are approximate upper bounds on the true error, i.e.

$$\|g\| \lesssim \|\hat{g}\| \leq E_{\mathrm{est}}, \qquad \|g\| \lesssim \|\hat{g}\| \lesssim E_{\mathrm{est}}^{\Pi_{\mathrm{C}}}. \tag{99}$$

4.4. Summary of error estimation procedure

The steps to obtain the final expression in (98) are summarized below:

- Linearization of the error equation, cf. Eq. (55) and definition of the approximate error g;
- Definition of an auxiliary symmetric and bilinear form $\hat{A}_{\square}(\bullet, \bullet)$ that localizes in time, cf. Eq. (62), and the auxiliary error representation $\hat{g}$;
- Explicit residual based estimates of the terms in $\hat{A}_{\square}(\bullet, \bullet)$ (cf. sections 4.3.1, 4.3.2, and 4.3.3), with an extra POD based projection of the seepage term in the residual, cf. Eq. (82).

We emphasize once again that the estimate is approximate upper bound, since, due to the non-linearity of the problem, the following approximations were introduced in the derivations: linearization of the error equation, linearization around $p = 0$ when defining the auxiliary form $\hat{A}$, and assumption that $\|\Pi_{\mathrm{C}}\hat{g}\|_{\mathrm{a}} \leq \|\hat{g}\|_{\mathrm{a}}$.

5. Numerical examples

For the numerical examples we consider an RVE in three spatial dimensions consisting of gas saturated matrix material (phase 1) with spherical, water saturated, inclusions of two different types (phases 2 and 3, respectively), see Fig. 2. The material parameters for the three phases are presented in Table 1.

In order to quantify the sharpness of the error estimate (as compared to the exact error) we define the effectivity index as

$$\eta := \frac{E_{\mathrm{est}}}{E}, \tag{100}$$

where E_{est} is the estimate (Eq. (98)), and $E := \|p - p_{\mathrm{R}}\|$ the "exact" error.

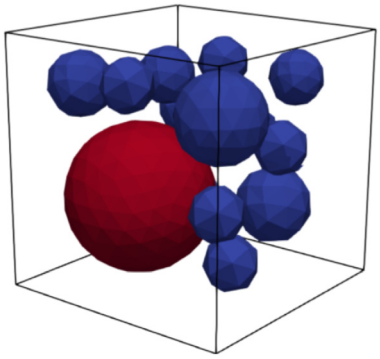

Fig. 2. RVE for the numerical examples with matrix Phase 1 matrix material (transparent) with spherical inclusions of Phase 2 (blue) and Phase 3 (red). (For interpretation of the references to color in this figure legend, the reader is referred to the web version of this article.)

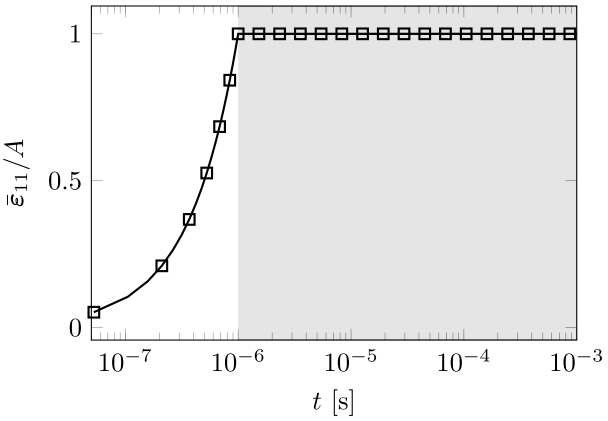

Fig. 3. Prescribed macroscale strain components used for training computations in the 11-direction, normalized with the amplitude A such that $\max_t \mathrm{tr}(\bar{\boldsymbol{\varepsilon}}(t)) = A$. The same loading is used for the 22- and 33-directions. Snapshots are collected during relaxation i.e. for $t > 1 \times 10^{-6}$ s.

5.1. Training computations for basis extraction

The reduced pressure basis is constructed using POD where snapshots are extracted from training computations. For the training we use a stress-relaxation test by ramping up the macroscale strain $\bar{\boldsymbol{\varepsilon}}_{11}(t)$, cf. Fig. 3, while keeping the other components fixed to 0 (and similarly for $\bar{\boldsymbol{\varepsilon}}_{22}(t)$ and $\bar{\boldsymbol{\varepsilon}}_{33}(t)$). Three different amplitudes of the loading $A = 0.01$, $A = 0.1$, and $A = 0.2$ are considered, resulting in three different profiles for the pore pressure, see Fig. 4. In order to quantify the magnitude of the non-linearity, the volume average of the permeability coefficient introduced in Eq. (8) is shown in Fig. 5.

The snapshots are collected from the "relaxation part" of the simulation, e.g. from the time steps where $t > 1 \times 10^{-6}$ s. From the snapshot dataset, with snapshots from all three training simulations, the POD basis is extracted as described in Section 3.4. In Fig. 6 the first pressure mode, p_1, and the corresponding displacement mode, $\boldsymbol{u}_1^{\mu}$ are visualized.

5.2. Example 1: Reduced solution of training simulations

As a first example we consider the macroscopic loading used for the training (see Section 5.1) and try to replicate the training simulations using the reduced basis. The result are presented for different magnitudes A, and for different tolerances used as the cutoff in the "residual-shifting" POD basis for the seepage w_t, see Section 4.3.2, i.e. $\lambda_M/\lambda_1 < \mathrm{TOL}$ where M determines the resulting number of modes. The seepage POD is based on snapshots from the reduced simulation. In Figs. 7 the number of seepage modes M are visualized for different N_{R} and for the

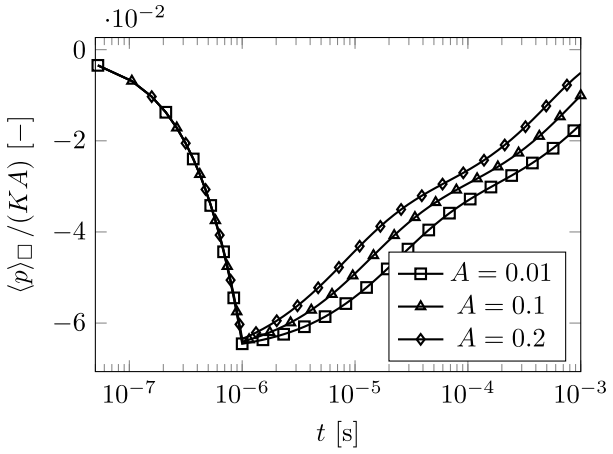

Fig. 4. Volume-averaged pressure $\langle p \rangle_\square$, normalized with the bulk modulus K and the amplitude A, corresponding to the macroscopic loading given in Fig. 3 for three different amplitudes.

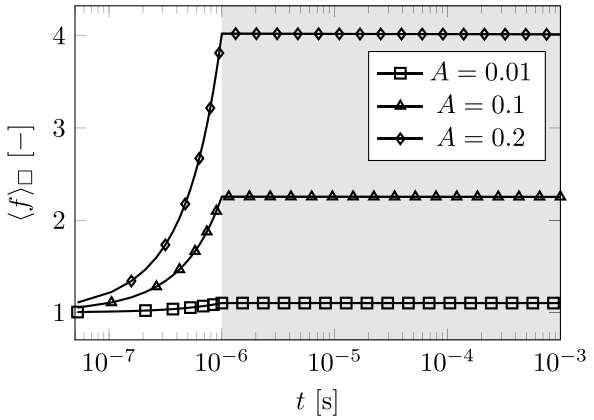

Fig. 5. Volume-averaged permeability coefficient $\langle f \rangle_\square$, corresponding to macroscopic loading given in Fig. 3, for three different amplitudes A.

different loading amplitudes A. The exact error and the estimate and the resulting effectivity index η are plotted in Figs. 8 and 9 for $A = 0.01$, in Figs. 10 and 11 for $A = 0.1$, and in Figs. 12 and 13 for $A = 0.2$. We note that as the amplitude increases the exact error (and the estimates) also increases, i.e. the basis performs worse for higher non-linearities. The figures show the importance of the residual shifting POD: using a better basis, in this case using a lower tolerance leading to more modes, have a significant impact on the estimate and the effectivity index.

5.3. Example 2: Combined macroscopic loading

In order to test the effectiveness of the reduced basis we also try a different macroscopic loading where the macroscopic strains $\bar{\varepsilon}_{11}$, $\bar{\varepsilon}_{22}$, and $\bar{\varepsilon}_{33}$ are varied according to Fig. 14. The same amplitudes used for the training is also used to define this loading ($A = 0.01$, $A = 0.1$, and $A = 0.2$), where each amplitude approximately corresponds to same maximum averaged pressure $\langle p \rangle_\square$, see Fig. 15, and the same maximum averaged permeability $\langle f \rangle_\square$, see Fig. 16.

The exact and estimated error in energy norm is plotted in Fig. 17 for $A = 0.01$, in Fig. 18 for $A = 0.1$, and in Fig. 19 for $A = 0.2$. In this example only the POD threshold $\lambda_M/\lambda_1 < 10^{-12}$ is used for the seepage basis. The figures also include results from the bound given in Eq. (72), i.e. the estimate is scaled with $f^- =$

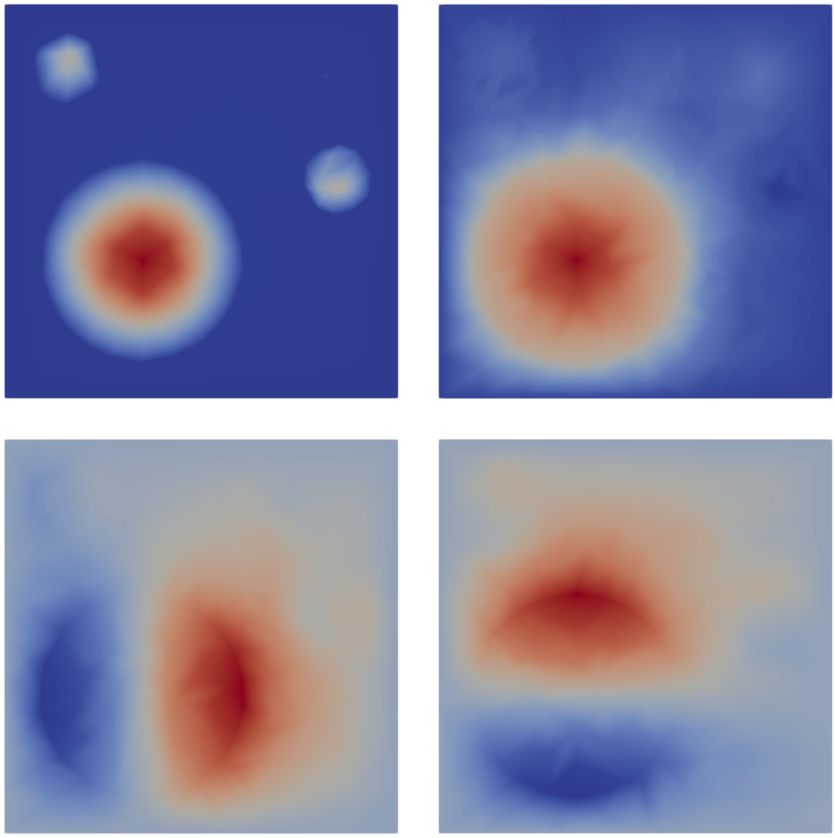

Fig. 6. The first mode shapes visualized on the yz-plane in the middle of the RVE: $p_1(\boldsymbol{x})$ top left, $\boldsymbol{u}^{\mu}_{1,x}(\boldsymbol{x})$ top right, $\boldsymbol{u}^{\mu}_{1,y}(\boldsymbol{x})$ bottom left, and $\boldsymbol{u}^{\mu}_{1,z}(\boldsymbol{x})$ bottom right.

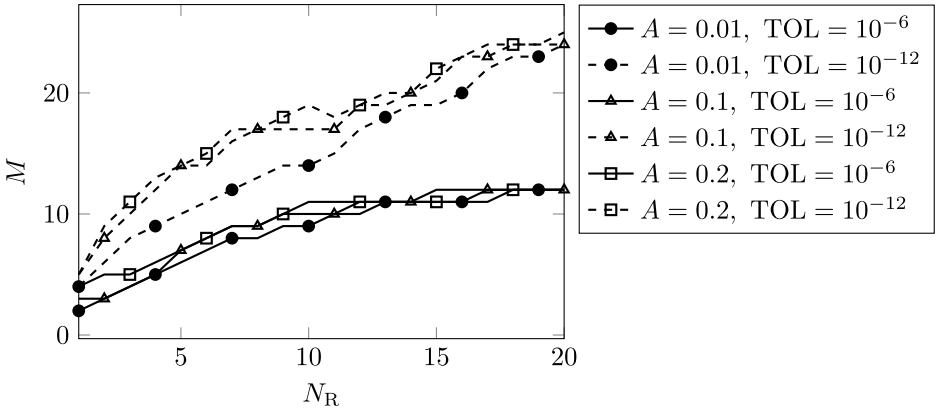

Fig. 7. *Example-1*: Number of seepage modes M obtained in the seepage POD, for the different tolerances and the different amplitudes A, as a function of number of modes N_{R} used for the pressure approximation.

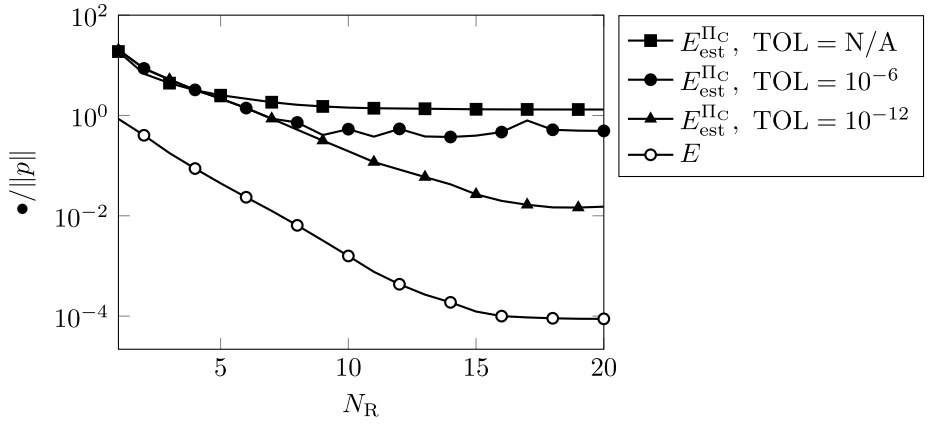

Fig. 8. *Example-1*: Exact and estimated error in energy norm for amplitude $A = 0.01$, for different tolerances for generating the seepage POD basis in the residual shifting.

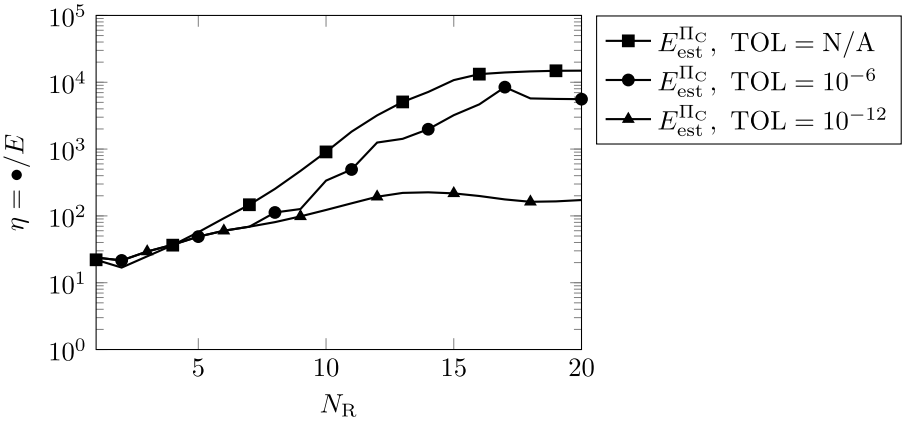

Fig. 9. *Example-1*: Effectivity index for the estimated error in energy norm for $A = 0.01$, for different tolerances for generating the seepage POD basis in the residual shifting.

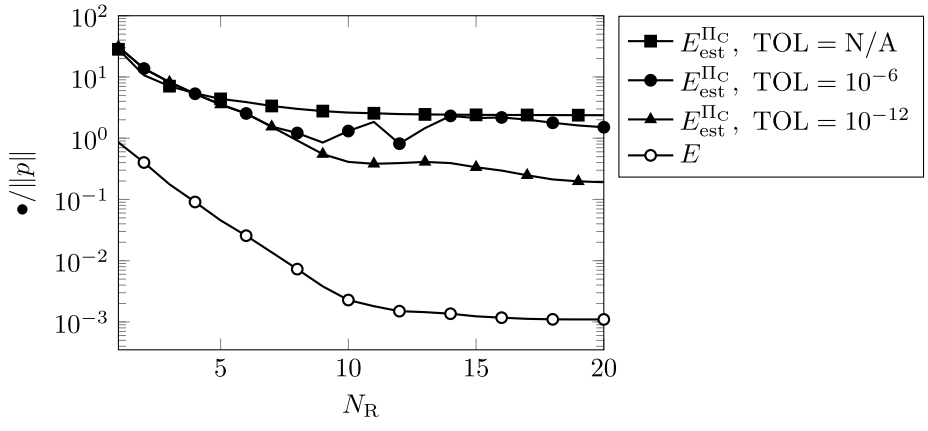

Fig. 10. *Example-1*: Exact and estimated error in energy norm for amplitude $A = 0.1$, for different tolerances for generating the seepage POD basis in the residual shifting.

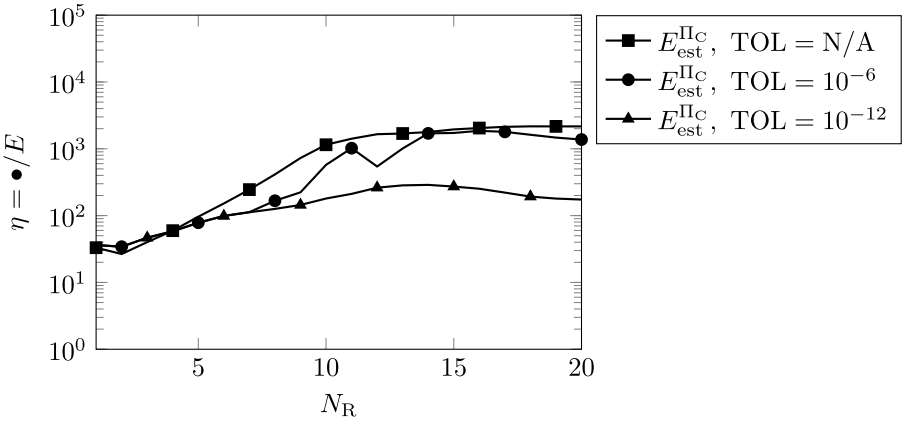

Fig. 11. *Example-1*: Effectivity index for the estimated error in energy norm for $A = 0.1$, for different tolerances for generating the seepage POD basis in the residual shifting.

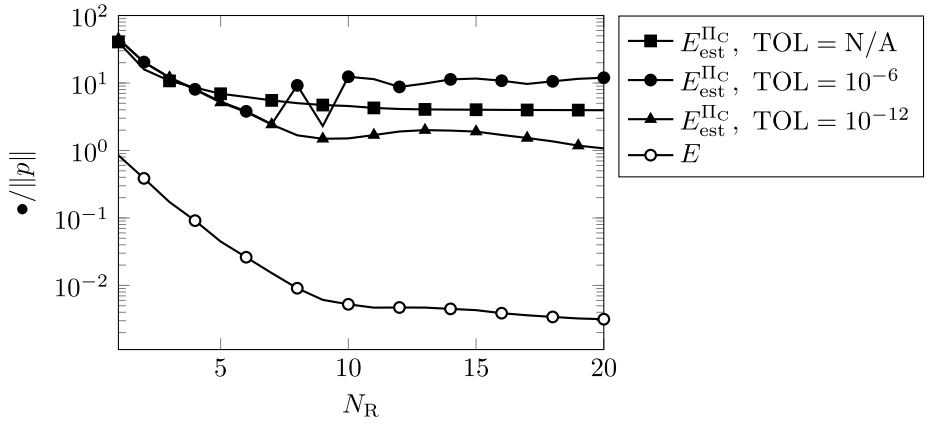

Fig. 12. *Example-1*: Exact and estimated error in energy norm for amplitude $A = 0.2$, for different tolerances for generating the seepage POD basis in the residual shifting.

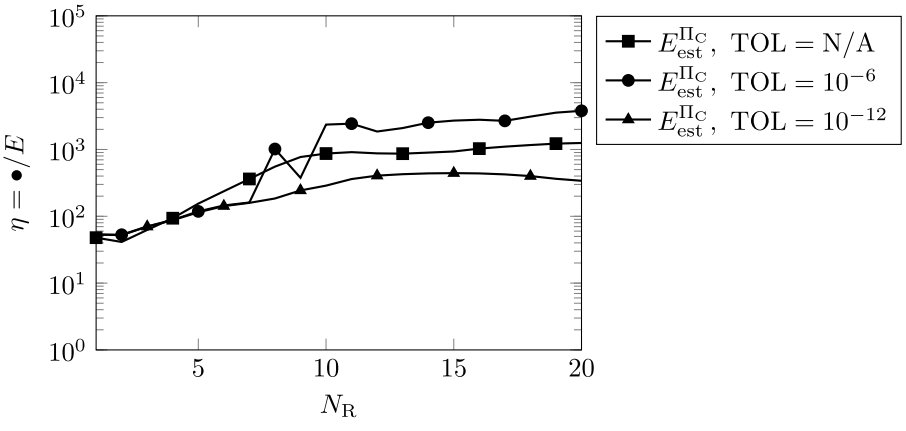

Fig. 13. *Example-1*: Effectivity index for the estimated error in energy norm for $A = 0.2$, for different tolerances for generating the seepage POD basis in the residual shifting.

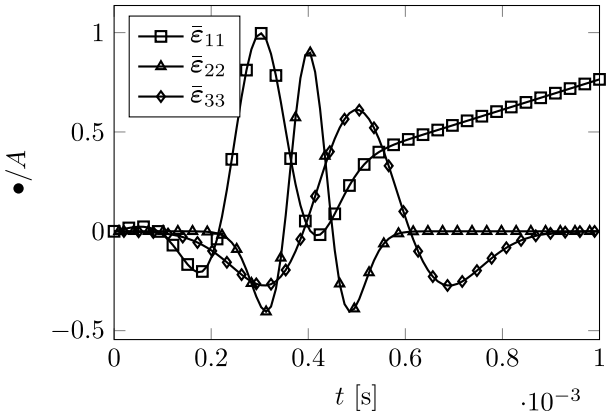

Fig. 14. *Example-2:* Prescribed macroscale strain components used for prediction normalized with the amplitude A such that $\max_t \mathrm{tr}(\bar{\boldsymbol{\varepsilon}}(t)) = A$.

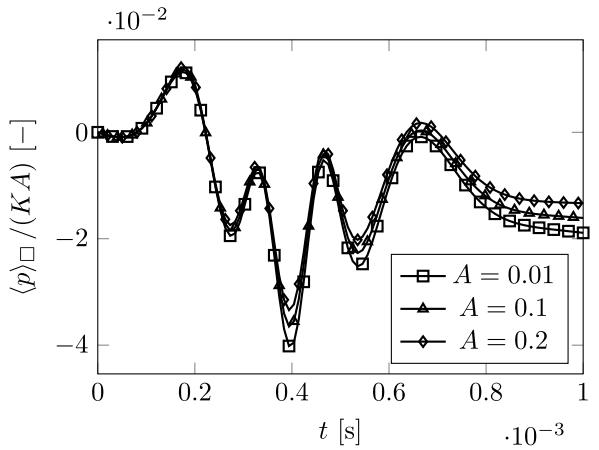

Fig. 15. *Example-2:* Volume-averaged pressure $\langle p \rangle_\square$, normalized with the bulk modulus K and the amplitude A, corresponding to the macroscopic loading given in Fig. 14, for three different amplitudes.

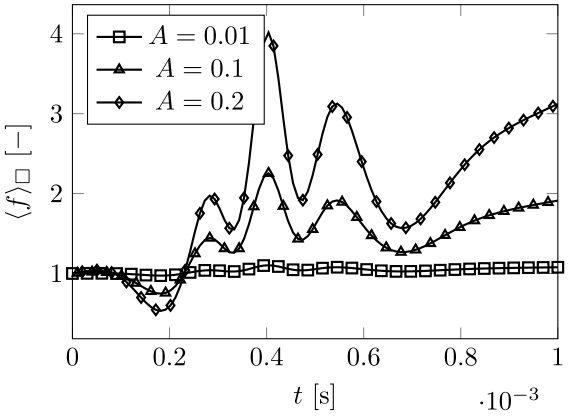

Fig. 16. *Example-2:* Volume-averaged permeability coefficient $\langle f \rangle_\square$ for the macroscopic load case given in Fig. 14, for three different amplitudes A.

$\min_{\boldsymbol{x} \in \Omega_\square, t \in I} f(\nabla \cdot \boldsymbol{u}(\boldsymbol{x}, t))$. However, we note the estimate is robust also without this, and, since f^- locally becomes very small for the higher amplitude loads, the resulting effectivity is very poor.

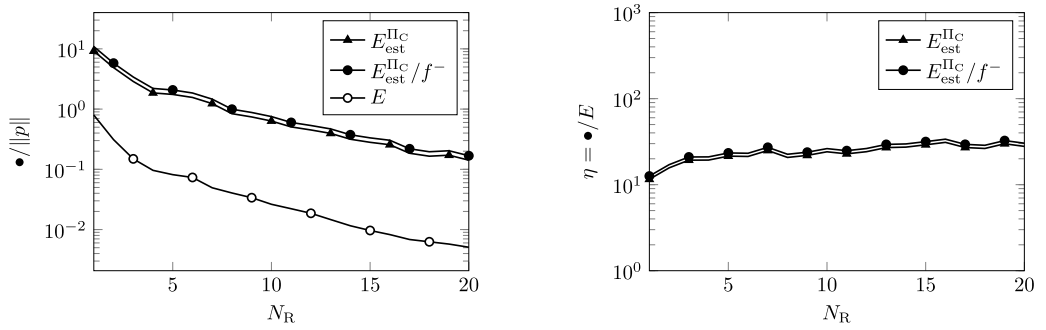

Fig. 17. *Example-2*: Exact and estimated error in energy norm (left) and effectivity index (right) using amplitude $A = 0.01$. The more conservative estimator is obtained through scaling by the factor f^-.

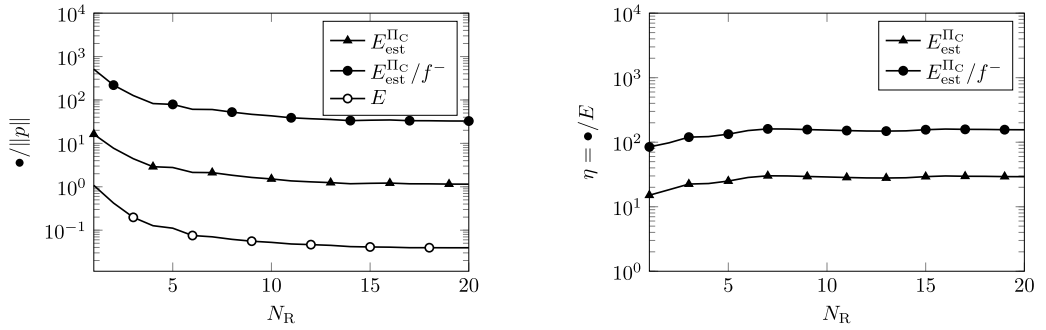

Fig. 18. *Example-2*: Exact and estimated error in energy norm (left) and effectivity index (right) using amplitude $A = 0.1$. The more conservative estimator is obtained through scaling by the factor f^-.

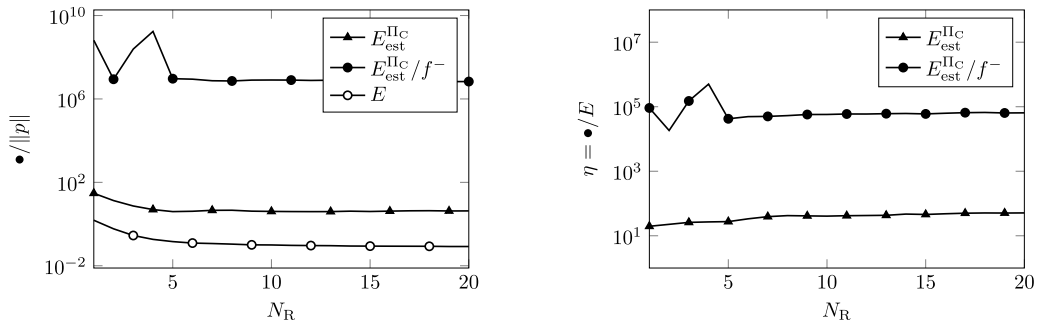

Fig. 19. *Example-2*: Exact and estimated error in energy norm (left) and effectivity index (right) using amplitude $A = 0.2$. The more conservative estimator is obtained through scaling by the factor f^-.

6. Conclusions and outlook

In this paper we have presented NMR applied to the RVE problem arising from computational homogenization of porous media with a non-linear constitutive relation for the seepage. We derived an explicit, fully computable, a posteriori error estimator based on the linearized error equation for estimation of the NMR error in terms of the energy norm pertinent to the linearized problem. The results for the chosen numerical examples demonstrate the performance of the estimator and it was shown that the estimator overestimates the true error between one and two orders of magnitude. For the studied model problem, the estimator is conservative also for strong non-linearities.

As shown for the linear problem [26], the effectivity of the estimator can be improved by including spectral modes in the reduced basis. This should be investigated also for the non-linear problem. Left for future work is also to further develop the estimator for estimation of user-defined quantities of interest (cf. [26]), and the application of the estimator to a full-fledged nested FE^2 procedure (cf. [25]), which would require taking care of error transport between the two scales. Finally, the procedure can be applied to other important applications of non-linear transient problems, accounting for e.g. inelastic deformations.

Declaration of competing interest

The authors declare that they have no known competing financial interests or personal relationships that could have appeared to influence the work reported in this paper.

Acknowledgments

This research was supported by the Swedish Research Council (VR) under grants 2015-05422 and 2019-05080. For the numerical implementation we want to acknowledge the open source community: the implementation was written in the Julia programming language [34], in particular using the finite element toolbox Ferrite.jl [35] and the tensor library Tensors.jl [36]. Meshing was performed using Gmsh [37]. The computations were enabled by resources provided by the Swedish National Infrastructure for Computing (SNIC) at Chalmers Centre for Computational Science and Engineering (C3SE).

References

[1] F. Feyel, J.-L. Chaboche, FE2 multiscale approach for modelling the elastoviscoplastic behaviour of long fibre SiC/Ti composite materials, Comput. Methods Appl. Mech. Engrg. (ISSN: 0045-7825) 183 (3) (2000) 309–330, http://dx.doi.org/10.1016/S0045-7825(99)00224-8.

[2] A. Waseem, T. Heuzé, L. Stainier, M.G.D. Geers, V.G. Kouznetsova, Model reduction in computational homogenization for transient heat conduction, Comput. Mech. 65 (1) (2020) 249–266, http://dx.doi.org/10.1007/s00466-019-01767-3, (ISSN: 0178-7675, 1432-0924).

[3] E. Aggestam, F. Larsson, K. Runesson, F. Ekre, Numerical model reduction with error control in computational homogenization of transient heat flow, Comput. Methods Appl. Mech. Engrg. (ISSN: 0045-7825) 326 (2017) 193–222, http://dx.doi.org/10.1016/j.cma.2017.08.006.

[4] J. Fish, Z. Yuan, Multiscale enrichment based on partition of unity for nonperiodic fields and nonlinear problems, Comput. Mech. (ISSN: 1432-0924) 40 (2) (2007) 249–259, http://dx.doi.org/10.1007/s00466-006-0095-0.

[5] C. Oskay, J. Fish, On calibration and validation of Eigendeformation-based multiscale models for failure analysis of heterogeneous systems, Comput. Mech. (ISSN: 1432-0924) 42 (2) (2008) 181–195, http://dx.doi.org/10.1007/s00466-007-0197-3.

[6] Dvorak George J, Benveniste Yakov, On transformation strains and uniform fields in multiphase elastic media, Proc. R. Soc. Lond. Ser. A Math. Phys. Sci. 437 (1900) (1992) 291–310, http://dx.doi.org/10.1098/rspa.1992.0062.

[7] J.C. Michel, P. Suquet, Nonuniform transformation field analysis, Int. J. Solids Struct. (ISSN: 0020-7683) 40 (25) (2003) 6937–6955, http://dx.doi.org/10.1016/S0020-7683(03)00346-9, Special Issue in Honor of George J. Dvorak.

[8] J.C. Michel, P. Suquet, Computational analysis of nonlinear composite structures using the nonuniform transformation field analysis, Comput. Methods Appl. Mech. Engrg. (ISSN: 0045-7825) 193 (48) (2004) 5477–5502, http://dx.doi.org/10.1016/j.cma.2003.12.071, Advances in Computational Plasticity.

[9] F. Fritzen, T. Böhlke, Reduced basis homogenization of viscoelastic composites, Compos. Sci. Technol. (ISSN: 0266-3538) 76 (2013) 84–91, http://dx.doi.org/10.1016/j.compscitech.2012.12.012.

[10] F. Fritzen, M. Leuschner, Reduced basis hybrid computational homogenization based on a mixed incremental formulation, Comput. Methods Appl. Mech. Engrg. (ISSN: 0045-7825) 260 (2013) 143–154, http://dx.doi.org/10.1016/j.cma.2013.03.007.

[11] F. Fritzen, M. Hodapp, M. Leuschner, GPU accelerated computational homogenization based on a variational approach in a reduced basis framework, Comput. Methods Appl. Mech. Engrg. (ISSN: 0045-7825) 278 (2014) 186–217, http://dx.doi.org/10.1016/j.cma.2014.05.006.

[12] F. Fritzen, M. Leuschner, Nonlinear reduced order homogenization of materials including cohesive interfaces, Comput. Mech. (ISSN: 1432-0924) 56 (1) (2015) 131–151, http://dx.doi.org/10.1007/s00466-015-1163-0.

[13] R. Jänicke, F. Larsson, K. Runesson, H. Steeb, Numerical identification of a viscoelastic substitute model for heterogeneous poroelastic media by a reduced order homogenization approach, Comput. Methods Appl. Mech. Engrg. (ISSN: 0045-7825) 298 (2016) 108–120, http://dx.doi.org/10.1016/j.cma.2015.09.024.

[14] N.C. Nguyen, A multiscale reduced-basis method for parametrized elliptic partial differential equations with multiple scales, J. Comput. Phys. (ISSN: 0021-9991) 227 (23) (2008) 9807–9822, http://dx.doi.org/10.1016/j.jcp.2008.07.025.

[15] Y. Efendiev, J. Galvis, F. Thomines, A systematic coarse-scale model reduction technique for parameter-dependent flows in highly heterogeneous media and its applications, Multiscale Model. Simul. (ISSN: 1540-3459) 10 (4) (2012) 1317–1343, http://dx.doi.org/10.1137/110853030.

[16] Y. Efendiev, J. Galvis, E. Gildin, Local–global multiscale model reduction for flows in high-contrast heterogeneous media, J. Comput. Phys. (ISSN: 0021-9991) 231 (24) (2012) 8100–8113, http://dx.doi.org/10.1016/j.jcp.2012.07.032.

[17] J.A. Hernández, J. Oliver, A.E. Huespe, M.A. Caicedo, J.C. Cante, High-performance model reduction techniques in computational multiscale homogenization, Comput. Methods Appl. Mech. Engrg. (ISSN: 0045-7825) 276 (2014) 149–189, http://dx.doi.org/10.1016/j.cma.2014.03.011.

[18] A. Memarnahavandi, F. Larsson, K. Runesson, A goal-oriented adaptive procedure for the Quasi-continuum method with cluster approximation, Comput. Mech. (ISSN: 1432-0924) 55 (4) (2015) 617–642, http://dx.doi.org/10.1007/s00466-015-1127-4.

[19] A. Abdulle, Y. Bai, G. Vilmart, Reduced basis finite element heterogeneous multiscale method for quasilinear elliptic homogenization problems, Discrete Contin. Dyn. Syst. S2015 8 (2014) 91–118, http://dx.doi.org/10.3934/dcdss.2015.8.91, 65N30, 65M60, 74D10, 74Q05, http://www.aimsciences.org/journals/displayArticlesnew.jsp?paperID=10102.

[20] A. Abdulle, Y. Bai, Adaptive reduced basis finite element heterogeneous multiscale method, Comput. Methods Appl. Mech. Engrg. (ISSN: 0045-7825) 257 (2013) 203–220, http://dx.doi.org/10.1016/j.cma.2013.01.002.

[21] S. Boyaval, Reduced-basis approach for homogenization beyond the periodic setting, Multiscale Model. Simul. (ISSN: 1540-3459) 7 (1) (2008) 466–494, http://dx.doi.org/10.1137/070688791.

[22] M. Ohlberger, F. Schindler, Error control for the localized reduced basis multiscale method with adaptive on-line enrichment, SIAM J. Sci. Comput. (ISSN: 1064-8275) 37 (6) (2015) A2865–A2895, http://dx.doi.org/10.1137/151003660.

[23] P. Kerfriden, J.J. Ródenas, S.P.-A. Bordas, Certification of projection-based reduced order modelling in computational homogenisation by the constitutive relation error, Internat. J. Numer. Methods Engrg. (ISSN: 1097-0207) 97 (6) (2014) 395–422, http://dx.doi.org/10.1002/nme.4588.

[24] L. Chamoin, F. Legoll, A posteriori error estimation and adaptive strategy for the control of MsFEM computations, Comput. Methods Appl. Mech. Engrg. (ISSN: 0045-7825) 336 (2018) 1–38, http://dx.doi.org/10.1016/j.cma.2018.02.016.

[25] F. Ekre, F. Larsson, K. Runesson, On error controlled numerical model reduction in FE2-Analysis of transient heat flow, Internat. J. Numer. Methods Engrg. (ISSN: 1097-0207) 119 (1) (2019) 38–73, http://dx.doi.org/10.1002/nme.6041.

[26] F. Ekre, F. Larsson, K. Runesson, R. Jänicke, A posteriori error estimation for numerical model reduction in computational homogenization of porous media, Internat. J. Numer. Methods Engrg. 121 (23) (2020) 5350–5380, http://dx.doi.org/10.1002/nme.6504, (ISSN: 0029-5981, 1097-0207).

[27] N. Parés, P. Díez, A. Huerta, Bounds of Functional Outputs for Parabolic Problems. Part I: Exact Bounds of the Discontinuous Galerkin Time Discretization, Comput. Methods Fluid Struct. Interact., 197(19), 1641–1660, https://doi.org/10.1016/j.cma.2007.08.025, issn=0045-7825, Computer Methods in Applied Mechanics and Engineering.

[28] N. Parés, P. Díez, A. Huerta, Bounds of functional outputs for parabolic problems. Part II: Bounds of the exact solution, Comput. Methods Fluid Struct. Interact. (ISSN: 0045-7825) 197 (19) (2008) 1661–1679, http://dx.doi.org/10.1016/j.cma.2007.08.024, Computer Methods in Applied Mechanics and Engineering.

[29] N. Parés, P. Díez, A. Huerta, Exact bounds for linear outputs of the advection-diffusion-reaction equation using flux-free error estimates, SIAM J. Sci. Comput. (ISSN: 1064-8275) 31 (4) (2009) 3064–3089, http://dx.doi.org/10.1137/080724356.

[30] H. Jakobsson, F. Bengzon, M.G. Larson, Adaptive component mode synthesis in linear elasticity, Internat. J. Numer. Methods Engrg. (ISSN: 1097-0207) 86 (7) (2011) 829–844, http://dx.doi.org/10.1002/nme.3078.

[31] M.A. Biot, General theory of three-Dimensional Consolidation, J. Appl. Phys. (ISSN: 0021-8979) 12 (2) (1941) 155–164, http://dx.doi.org/10.1063/1.1712886.

[32] J.R. Rice, M.P. Cleary, Some basic stress diffusion solutions for fluid-saturated elastic porous media with compressible constituents, Rev. Geophys. (ISSN: 8755-1209) 14 (2) (1976) 227, http://dx.doi.org/10.1029/RG014i002p00227.

[33] F. Larsson, K. Runesson, F. Su, Variationally consistent computational homogenization of transient heat flow, Internat. J. Numer. Methods Engrg. (ISSN: 1097-0207) 81 (13) (2010) 1659–1686, http://dx.doi.org/10.1002/nme.2747.

[34] J. Bezanson, A. Edelman, S. Karpinski, V. Shah, Julia: A fresh approach to numerical computing, SIAM Rev. (ISSN: 0036-1445) 59 (1) (2017) 65–98, http://dx.doi.org/10.1137/141000671.

[35] K. Carlsson, F. Ekre, contributors, Ferrite.jl – Finite element toolbox for Julia, URL: https://github.com/Ferrite-FEM/Ferrite.jl.

[36] K. Carlsson, F. Ekre, Tensors.jl – tensor computations in julia, J. Open Res. Softw. (2019) http://dx.doi.org/10.5334/jors.182.

[37] C. Geuzaine, J.-F. Remacle, Gmsh: A 3-D finite element mesh generator with built-in pre- and post-processing facilities, Internat. J. Numer. Methods Engrg. (ISSN: 1097-0207) 79 (11) (2009) 1309–1331, http://dx.doi.org/10.1002/nme.2579.